Semi-empirical water dimer model of the water vapour self-continuum within the IR absorption bands

Semi-empirical water dimer model of the water vapour self-continuum within the IR absorption bands

Anna A. Simonova[a], Igor V. Ptashnik[a], Keith P. Shine[b]

[a] Atmospheric Spectroscopy Division, V.E. Zuev Institute of Atmospheric Optics SB RAS, Tomsk, 1 Academician Zuev square, 634055, Russia
[b] Department of Meteorology, University of Reading, Reading, RG66ET, UK

E-mail addresses: saa@iao.ru, piv@iao.ru, k.p.shine@reading.ac.uk

Corresponding author: Igor V. Ptashnik (piv@iao.ru)

Abstract

Water vapour continuum absorption is an important component of atmospheric radiative transfer codes. It significantly impacts the radiative balance of the atmosphere, but the physical nature of this absorption remains a subject of discussion. Here the H_2O self-continuum absorption is considered within the infrared absorption bands (from 50 to 11 200 cm^{-1}) of water vapour exploiting existing measurements. Comparison of this data with the MT_CKD-3.5 continuum model, which is used in many radiative transfer codes, reveals significant quantitative and qualitative differences. New water vapour self-continuum spectra are derived from earlier FTS measurements using HITRAN-2016 in the 5300 and 7200 cm^{-1} bands. A previously proposed water dimer model is refined and unified based on a broad set of up-to-date experimental data on the H_2O continuum. The new model, which is suitable for incorporation into radiative transfer codes, has a much firmer physical basis than existing models. It reproduces the spectral behaviour and magnitude of the in-band water vapour self-continuum for temperatures from 279 to 431 K depending on the band. Importantly, the fitted total equilibrium dimerization constant used in the updated continuum model exceeds independent estimates by a factor of 1.5–3 across the entire temperature and spectral regions studied. Possible causes for this, which are important for understanding the physical origin of the continuum, are discussed. The contribution of water dimer to the continuum is estimated to vary from 40 to 90% depending on absorption band and temperature.

Keywords: continuum absorption, water vapour, absorption band, water dimer, line wing, semi-empirical model

1. Introduction

Water vapour, being the main absorber of solar radiation and the strongest greenhouse gas in the Earth's atmosphere, is a high priority in studies of the atmosphere and climate. Water vapour determines most of the atmospheric absorption from microwave to visible frequencies. The infrared (IR) spectral region, which includes the maximum outgoing heat flux of the

Earth and the strongest absorption of solar radiation by water vapour, is of particular interest from the point of view of radiative balance of the atmosphere and its impact on climate change. The water vapour absorption spectrum in this region is a series of absorption bands separated by atmospheric windows.

There are two conventionally distinguished components of the water vapour absorption spectrum. The first one is *selective* (or *resonance*) absorption, which is determined by a cumulative contribution of water monomer spectral lines. At present, parameters of a large number of H_2O spectral lines are known with high accuracy from quantum-chemical calculations and experiments and can be used to simulate the selective absorption spectrum in wide frequency regions and thermodynamic conditions. These parameters are available in open spectroscopic databases such as HITRAN [1], GEISA [2], etc.

The second component of the water vapour absorption spectrum is the so-called *continuum* absorption characterized by a much weaker dependence on frequency than absorption by spectral lines. The continuum absorption is defined as a difference between the water vapour experimental absorption and the simulated selective absorption spectra. The water vapour continuum was first discovered in the transparency window of 8–14 μm about a century ago [3]. Nevertheless, the nature of this phenomenon still remains insufficiently studied and understood. The importance of the continuum for the atmospheric radiation budget has been the subject of many studies (e.g. [4–6]). The continuum is also relevant in many remote sensing applications (e.g., [7]). The water vapour continuum consists of two components: the so-called *self*- and *foreign*-continua, resulting from the interactions of H_2O molecules with each other and H_2O molecules with molecules of other atmospheric gases, respectively. This work considers the water vapour self-continuum. Within atmospheric windows, the water vapour self-continuum absorption is, in a wavenumber integrated sense, greater than the weak monomer lines by an order of magnitude or even more, and has a spectral structure that varies smoothly with frequency. In these windows, the water vapour continuum plays the most important role in the radiative balance of the atmosphere [4,8].

Within the IR absorption bands, the continuum is 2–3 orders of magnitude weaker than the selective absorption at spectral line centres; however, is quite comparable with this absorption in microwindows, i.e. between H_2O spectral lines. Within bands, the water vapour continuum spectrum remains less studied today compared to the atmospheric windows, probably due to its relatively minor applied interest. The first laboratory-based experimental data on the water vapour continuum within the IR bands were obtained only in the 1980s in the bands centred at1600 cm^{-1} [9] and 3600 cm^{-1} [10]. However, the opportunity to obtain the reliable laboratory data on the in-band IR water vapour self-continuum became available at the beginning of the 21st century, when the requirements of high resolution (comparable to the average line half-width and higher) of experimental data and low uncertainties in the spectral line parameters for calculating the selective absorption had been achieved For the in-band continuum, a key aspect is that it has characteristic broad spectral features – absorption peaks – which are of particular importance for understanding physical mechanisms responsible for the continuum absorption. In addition, even earlier experimental continuum data are known [11,12], obtained in the high-frequency wing of the rotational absorption band from 333 to 633 cm^{-1}. However, the continuum in this spectral region is difficult to interpret as

in-band, since the data are located in the wing of the band and do not have spectral features that are so important in the framework of this study.

From afundamental point of view, the water vapour continuum is interesting for understanding the understudied properties of the H_2O molecule in the gas phase. In particular, the continuum spectrum contains information on the effects that arise from intermolecular interactions of H_2O molecules in a real gas: "non-Lorentzian" wings of H_2O spectral lines resulting from the specifics and finite duration of water molecules collisions (the hypothesis of water monomer line wings, starting with [13]) and the formation of short-lived pair states of H_2O molecule with characteristic absorption spectra (the hypothesis of water dimers[1], starting with [14,15], later including in the bimolecular absorption hypothesis [16]).

Within the IR absorption bands, the water dimer hypothesis of the continuum is of particular importance. The water dimer absorption spectrum is determined by a sum of spectral lines corresponding to rovibrational transitions in water dimers. Due to the large number of vibrational degrees of freedom (12 *versus* 3 in water molecule), the water dimer has a much greater number of allowed transitions compared to the H_2O monomer. Thus, the water dimer spectral lines overlap strongly, forming an unresolved spectral structure (except at very cold temperatures). Within the absorption bands, this structure consists of some *subbands* corresponding to different vibrational transitions in water monomer units within the dimer. The corresponding absorption peaks were found in the experimental continuum absorption spectra within the IR bands (see references in Section 2). The observed structural similarities drew the attention of researchers to the probable contribution of water dimer absorption to the water vapour continuum spectrum [17–22]. A detailed description of the history of the study of the water vapour continuum absorption can be found in [23,24]. The motivation for the present study is the still open fundamental question about the origin of the continuum absorption and the emergence of new experimental and theoretical data on the water vapour absorption which allows the development of a more refined model of the in-band continuum, suitable for incorporation in radiative transfer codes.

In some cases, knowledge of the magnitude of the self-continuum within absorption bands enables the refinement of the water monomer spectral line parameters or detection of errors in spectral databases (see, for example, [25,26]), which in turn also affects the accuracy of atmospheric absorption simulations. Also, reliable information on the value and spectral features of the self-continuum absorption makes possible a more accurate retrieval of the foreign-continuum absorption(see, for instance, [27]). The water vapour foreign-continuum absorption along with the self-continuum contributes to the atmospheric absorption and must be accounted for in calculations of the radiative balance of the atmosphere.

To this day, the Mlawer-Tobin_Clough-Kneizys-Davies (MT_CKD) semi-empirical continuum model [28] has, in general, proved itself to be a reasonable solution for simulation of the water vapour continuum spectra in many spectral

[1] Water dimer is a molecular complex consisting of two H_2O monomers associated by a hydrogen (or Van der Waals) bond.

intervals within the spectral region from 0 to 20000 cm^{-1} including both the IR bands and atmospheric windows. A description of the MT_CKD model can be found in [28], and its updates can be tracked on the website [29]. This model is widely used in simulations of atmospheric radiative transfer. However, despite its general effectiveness in atmospheric windows, within the water vapour absorption bands, notable qualitative and quantitative differences between the MT_CKD model and experimental data on the continuum absorption have been found (some examples are presented in this paper). It is obvious today that some part of the continuum absorption in the MT_CKD model can be attributed to the water dimer absorption. So, the current investigation is intended to help to separate this part and thus to improve accuracy and physical background of the water vapour continuum model leading to an improved representation of the water vapour continuum in atmospheric radiative transfer models.

In our earlier works, the latest experimental data on the water vapour self-continuum absorption and preliminary estimates of the integrated contribution of water dimer absorption to the continuum, using a water dimer continuum model [22] and the then most-recent spectroscopic data, were presented; this covered the rotational [26,30] and rovibrational IR absorption bands centred near 1600 and 3600 cm^{-1} [31–33] and 8800 and 10 600 cm^{-1} [34]. In the present work, the continuum spectra were retrieved within the bands centred at 5300 cm^{-1} and 7200 cm^{-1} using experimental data from [31] and the HITRAN-2016 database [35]. This made it possible to collect the full set of the most recent data on the water vapour continuum absorption from experiments within the strongest IR bands located from 50 to 11 200 cm^{-1}. The purpose of this work is to analyse the possible contribution of water dimers to the water vapour continuum spectra within the IR bands in extended spectral and temperature ranges, and to present a semi-empirical modification of the water dimer continuum model.

The paper structure is the following. Section 2 contains a brief description of the retrieval of the water vapour continuum spectra from high-resolution Fourier-transform spectrometry (FTS) spectra within the strongest IR absorption bands. In Sect. 3, the parameterization of the earlier suggested water vapour continuum dimer model [22] within the absorption bands studied here is considered. The discussion of the results is presented in Sect. 4. The newly developed semi-empirical *dimer-based* continuum model for the IR absorption bands is described in Sect. 5. Conclusions are summarized in Sect. 6. The newly retrieved water vapour continuum spectra within 5300 and 7200 cm^{-1} bands are given in the Appendix A. The spectra of the new semi-empirical *dimer-based* continuum model, as well as the estimated real equilibrium constants of bound and quasibound dimers, are shortly described in the Appendix B, presented in tabular form in the Supplementary material 1 and illustrated in the figures of the Supplementary material 2. The data in the Supplementary material 1 can be readily incorporated into atmospheric radiative transfer codes. Appendix C contains a description of the notation introduced by the authors related to the dimerization of water vapor.

2. Experimental data

Since the origin of the water vapour continuum absorption has not yet received a strict physical description, direct recording of the continuum is not available. The standard approach to obtaining experimental data on the water vapour continuum

includes usually three main stages: (1) measurement of (total) pure water vapour absorption spectra; (2) simulation of local absorption of the water monomer spectral lines with parameters from a spectroscopic database; (3) taking the difference of the spectra obtained in steps (1) and (2).

To date, there are laboratory-based experimental data on the water vapour self-continuum within almost all IR absorption bands (see Tables 1 and 2). The exception is for the weakest bands near 12200 cm^{-1}. To receive reliable absorption data in this band, more sensitive measurement techniques than FTS are required. For example, the cavity ring-down spectroscopy (CRDS)technique is relevant for this goal [36]. Table 1 lists a number of works devoted to the retrieval of the water vapour self-continuum spectra within the IR absorption bands, many of which used databases prior to HITRAN-2016 [35].

Table 1. Example of available experimental data on the in-band water vapour self-continuum absorption many of which used databases prior to HITRAN-2016 (see extension with latest data in Table 2).

Literature source	***T*, K**
150 cm^{-1}	
Burch (1979, 1982) [11,12]	296, 338, 430
Liebe et al. (1987) [37]	296
Kuhn et al. (2002) [38]	296-356
Podobedov et al. (2008) [39]	293, 313, 333
Koshelev et al. (2011) [40]	261-328
Slocum et al. (2015) [41]	296
Odintsova et al. (2017) [42]	297
Koshelev et al. (2018) [43]	296
Odintsova et al. (2019) [44]	297
1600 cm^{-1}	
Burch(1981) [9]	308
Tobin(1996) [45]	260, 296
Paynter et al. (2009) [31]	296, 330, 351
Ptashnik et al. (2013) [46]	288–289.5, 318
Ptashnik et al. (2016) [47]	268–289
3600 cm^{-1}	
Burch(1985) [10]	296
Paynter et al. (2007) [20]	296, 351
Paynter et al. (2009) [31]	296, 304, 317, 327, 337; 351
Ptashnik et al. (2013) [46]	288–289.5, 318
Ptashnik et al. (2016) [47]	268–289
Birk et al. (2020) [48]	296, 353
5300 cm^{-1}	
Ptashnik et al. (2004) [18]	297, 299, 342
Paynter et al. (2009) [31]	293, 317, 337, 351
Ptashnik et al. (2013) [46]	288–289.5, 318
7200 cm^{-1}	
Paynter et al. (2009) [31]	317, 337, 351
Ptashnik et al. (2013) [46]	288–289.5, 318

In this work, a wide set of recent experimental data on the water vapour self-continuum, retrieved using the HITRAN-2016 database [35], is investigated. For clarity, these data are presented in a separate table, Table 2. Within absorption bands,

the water vapour self-continuum is comparable with the selective absorption in many microwindows (i.e. in between spectral lines). Therefore, the retrieved continuum spectra within the bands largely depend on uncertainties in the spectral line parameters used for calculation of selective absorption spectra. Thus, the newer the spectroscopic database that is used to retrieve continuum spectra, the more reliable, in general, the obtained experimental in-band continuum can be considered. The most recent version of the HITRAN database is HITRAN-2020 [1]. Therefore, it is worth more clearly explaining the motivation for using HITRAN-2016 in this work.

First, the latest version – HITRAN-2020 [1] – became officially available only at the end of 2021, which was after the end of our data processing. However, this does not markedly affect our results. Only strong and middle intensity lines affect the retrieved in-band continuum absorption. Parameters of such lines (intensities and linewidths) did not change markedly during recent HITRAN updates, since many of them had already been studied in detail earlier. Therefore, the main differences between the retrieved continuum spectra using the HITRAN-2016 and HITRAN-2020 can be caused only by difference in parameters of relatively weak H_2O lines. The latter, in turn, have much less impact on the retrieved continuum. As an example, Fig. 1 shows continuum spectra retrieved using the 2016 and 2020 versions of HITRAN for a subset of data used here in several IR absorption bands at different temperatures. It can be seen that the use of a newer HITRAN version does not lead to any significant changes in the retrieved continuum values. Therefore, the data in Table 2 can still be considered reliable.

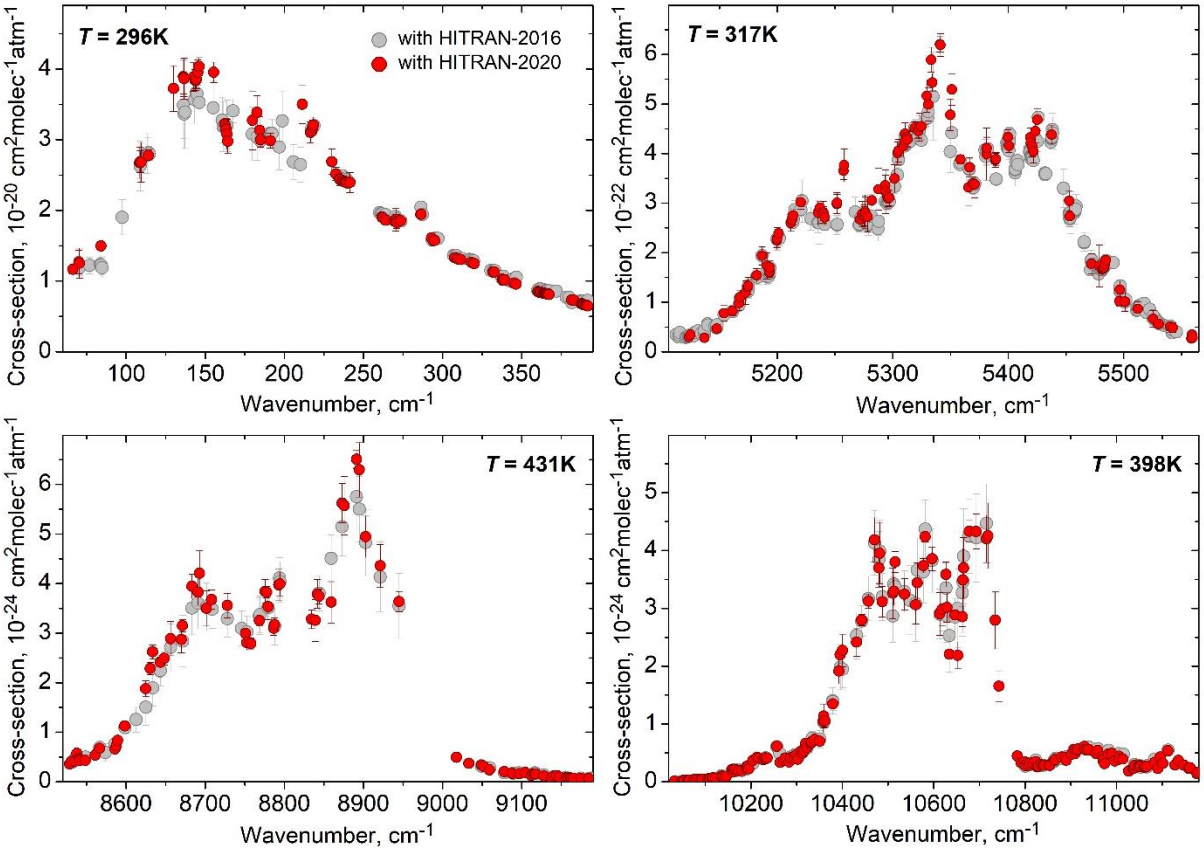

Fig. 1. The examples of the water vapour self-continuum spectra retrieved using the HITRAN-2016 [35] (grey circles) and HITRAN-2020 [1] (red circles) databases. The results are given for the experimental data presented in Table 2.

Second, one of the main results of this work is a new semi-empirical continuum model. The development of the universal model requires experimental data on the water vapour self-continuum in wide spectral and temperature ranges. Moreover, this has to be retrieved using a single version of the spectroscopic database. At the time of the development of the semi-empirical continuum model described in Sect. 5, the authors of this work and their colleagues (see links to works in Table 2) had completed the preparation of a set of 24 experimental water vapour continuum spectra retrieved with HITRAN-2016.

The more recent papers describe retrievals of the self-continuum spectra from the measurements of pure water vapour absorption within rotational and rovibrational IR bands in a wide temperature range of 279–431 K using HITRAN-2016 is presented in Table 2.

These measurements were carried out using Bruker IFS 125-HR Fourier Transform spectrometers (FTS) and multipass absorption cells at the Rutherford Appleton Laboratory (UK), at the Institute of Atmospheric Optics SB RAS (Russia), and the Synchrotron SOLEIL Facility (France). The experimental conditions are also presented in Table 2. The experimental optical depth of pure water vapour absorption $\tau_{exp}(\nu,T)$ at wavenumber ν and temperature T was derived according to the Beer–Lambert law:

$$\tau(\nu,T) = -\ln\left\{\frac{I(\nu,T)}{I_0(\nu,T)}\right\}, \quad (1)$$

where $I(\nu,T)$ and $I_0(\nu,T)$ are the FTS signals recorded when the absorption cell is filled with water vapour and evacuated (or filled with argon), respectively.

175

Table 2. Experimental conditions for the measurements of pure water vapour absorption within the IR absorption bands, from which the up-to-date H_2O self-continuum spectra were retrieved using the HITRAN-2016.

Absorption bands centred at, cm^{-1}	Literature source	Temperature, K	Pressure, mbar	Spectral resolution, cm^{-1}	Optical path length, m
150	Odintsova et al. (2020) [26]	296, 326	4–16	0.02	151.75
1600	Ptashnik et al. (2019) [32]	296–351	13.5–91	0.03	17.7
		278.8–288.4	6.4–11.5	0.01	28.8
3600	Ptashnik et al. (2019) [32]	296–351	12.1–156	0.03	17.7
		278.8–288.4	6.4–11.5	0.01	28.8
5300, 7200	Data from Paynter et al. (2009) [31] updated here using HITRAN-2016 (see Fig. 2 and Appendix A)	317, 336, 351	60–200	0.03	17.7
8800, 10 600	Simonova et al. (2022) [34]	398	1000–1370	0.1–0.2	17.7
		431	1080–2100	0.1–0.2	17.7
		431	3145–4155	0.4	9.7

To simulate the selective absorption spectra, a*line-by-line* code was used [49]. Each Voigt (for the rovibrational bands)
180 and Van Vleck–Huber (for the rotational band) line was calculated within 25 cm^{-1} from its centre without the "CKD-plinth" (see, for instance, Fig. 3 in [5]). The distance of 25 cm^{-1} (750 GHz) from the line centre is the classic cut-off boundary determining the range of the impact approximation [50]. This conventional approach to retrieving the continuum spectra gives the possibility of comparing correctly the continuum data obtained from different experimental studies and from simulations using the widely used MT_CKD continuum model [28]. The water vapour spectral line parameters were taken
185 from HITRAN-2016database [35].

At the final stage, the water vapour continuum optical depth $\tau_{cont}(\nu)$ was derived as a difference between the experimental water vapour optical depth spectrum $\tau_{exp}(\nu)$ and the calculated cumulative local contribution of water monomer lines $\tau_{mon}(\nu)$

$$\tau_{cont}(\nu) = \tau_{exp}(\nu) - \tau_{mon}(\nu). \quad (2)$$

The key stage in the retrieval procedure is the exclusion of wavenumbers near the centre of spectral linesfrom the processing,
190 where the uncertainty in the simulated local lines absorption is large compared to the continuum absorption. Thus, the experimental data on the water vapour continuum absorption is determined only at wavenumbers within microwindows between spectral lines. The following semi-empirical equation is used to describe the experimental self-continuum optical depth:

$$\tau_{cont}(\nu, P_s, T, L) = \alpha_{cont}(\nu, P_s, T)L = C_s(\nu, T)\rho_s P_s L = C_s(\nu, T)\frac{P_s^2 L}{kT}, \quad (3)$$

where ν, P_s, T and L are wavenumber, water vapour pressure, temperature and optical path length, respectively; α_{cont} is the continuum absorption coefficient [cm^{-1}]; C_s is the self-continuum cross-section [cm^2 molec^{-1} atm^{-1}]; ρ_s is the water vapour number density; k is the Boltzmann constant.

Approximation of the experimental dependence of the continuum absorption coefficients α_{cont} on pressure-squared by a linear function provides values of the self-continuum cross-sections C_s. Based on the results of this procedure, only reliable data for which the characteristic dependence of the water vapour continuum on water vapour pressure ($\alpha_{cont} \propto P_s^2$) is confirmed are selected. The detailed description of the retrieval procedure can be found elsewhere [26,34].

For joint analysis of experimental in-band continuum in the entire IR spectral region (excluding the unexplored 12 200 cm^{-1} absorption band), we also present here the newly retrieved water vapour self-continuum absorption within the 5300 and 7200 cm^{-1} absorption bands from the experimental data [31], using the HITRAN-2016[35] and a more sophisticated data-filtering technique realized in a specialized software for processing experimental data [51]. Since the most recent continuum retrievals in these bands were carried out more than a decade ago ([31] and [46]), it was necessary to update these data taking into account the newer database. The obtained self-continuum cross-sections C_s at 317, 336, and 351 K are presented in Fig. 2 and given in Appendix A. The characteristic H_2O pressure squared dependence and strong negative temperature dependence of the water vapour self-continuum absorption are found in this new analysis.

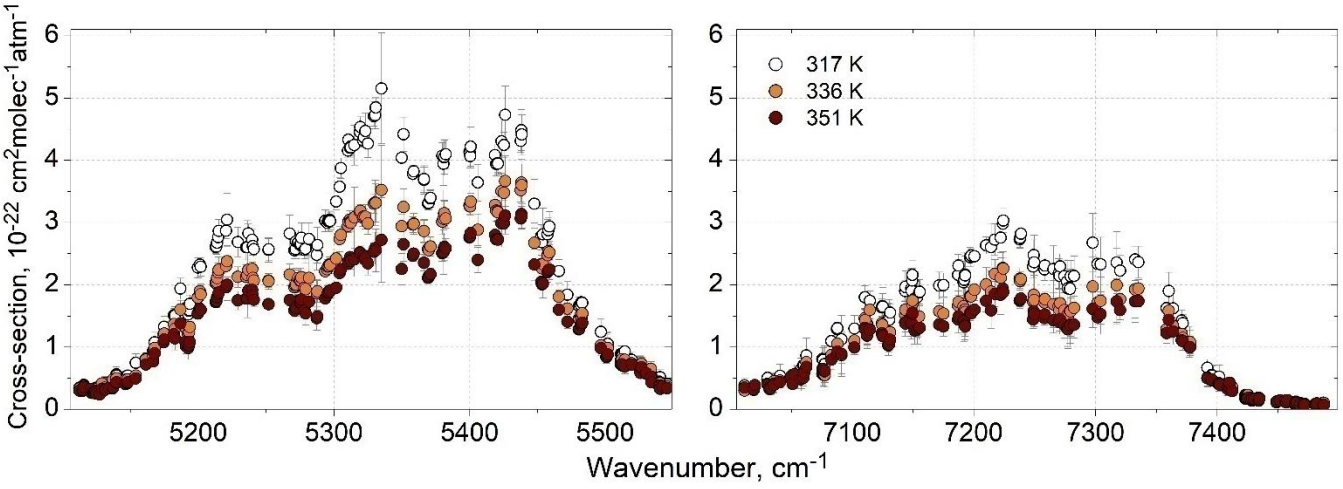

Fig. 2. Cross-section spectra of the water vapour self-continuum absorption retrieved from experiment [31] at 317 K (empty circles), 336 K (orange circles) and 351 K (dark red circles). The retrieval uncertainty is illustrated for data at 317 K only. The same information for 336 and 351 K is presented in Appendix A.

Experimental in-band water vapour self-continuum spectra located in the spectral region from 50 to 11 200 cm^{-1} (see examples in Fig. 3) are used here. All experimental spectra are obtained with the "CKD-plinth" included in the continuum

for direct comparison with the MT_CKD model. In this study, we use the MT_CKD-3.5 version, since there are no changes to the in-band continuum between 3.5 and the latest versions – 4.1 (see e.g. Fig. 2(d) in [28]) and 4.2 (see description in [29]).

For all the bands studied, a significant spectral difference between the experimental data and MT_CKD-3.5 continuum model, especially near the band centres, can be seen in Fig. 3. In particular, the MT_CKD model does not reproduce the observed experimental absorption peaks, which, in turn, play a key role in studying the origin of the in-band continuum absorption. Since the MT_CKD is primarily intended for application at atmospheric temperatures, a significant quantitative difference between the model and experiment at elevated temperatures can be explained by the limitations of the model. However, the spectral structure of the continuum should be reflected more realistically in the model at any temperature. To date, in all IR absorption bands, except for the bands centred near 12 200 cm^{-1}, there are experimental data on the water vapour self-continuum, which can be used to update MT_CKD.

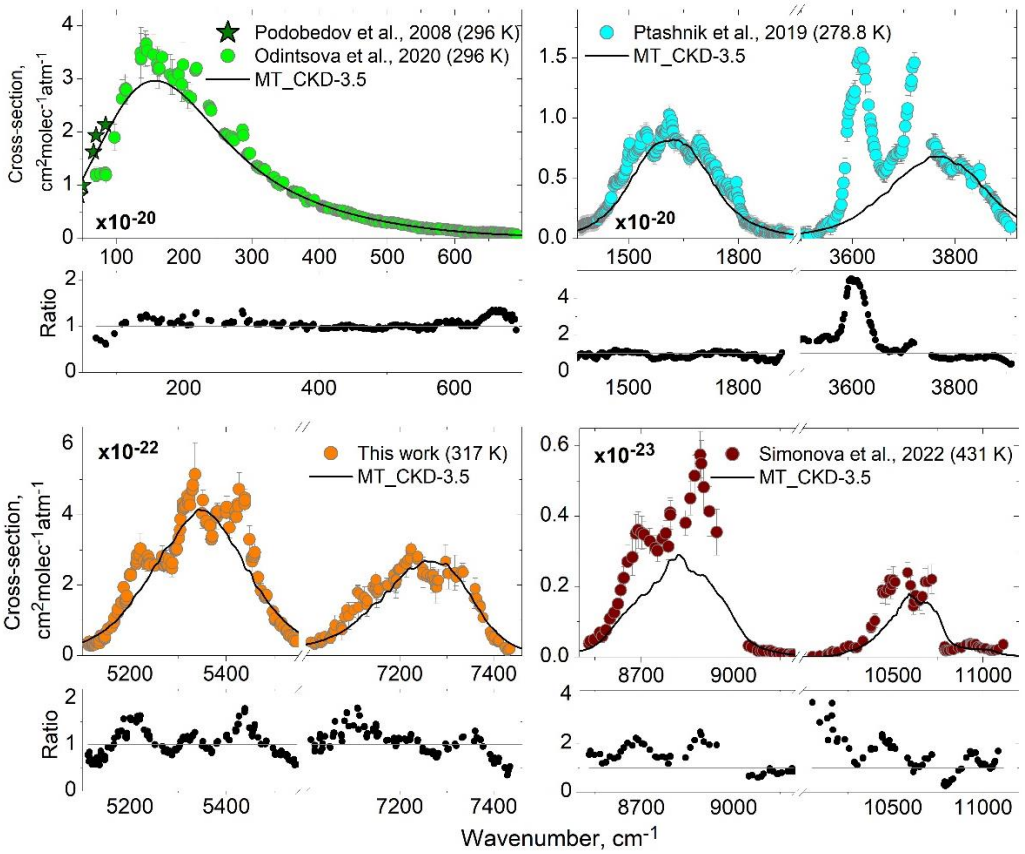

Fig. 3. Water vapour self-continuum cross-sections within all investigated to date IR absorption bands: examples of the experimental spectra (circles and stars) and the MT_CKD-3.5 model at the same temperatures (black curve). Ratios of the experimental water vapour self-continuum spectra to the MT_CKD-3.5 model are also shown in the lower panels.

The narrow lower panels in Fig. 3 show the ratios of the experimental values of the water vapour self-continuum to the MT_CKD model. The lowest maximum deviation (by a factor of ~1.4) is observed for the rotational absorption band. This is expected since the MT_CKD-3.5 update was carried out using the experimental data from Odintsova et al. [26] which is also used here. In the other absorption bands, this difference is greater (up to a factor of 5, for example, near 3600 cm^{-1}) both at atmospheric and elevated temperatures. Refinement of the spectral behavior of the MT_CKD model, taking into account the up-to-date experimental data, will obviously minimize the observed quantitative difference.

3. Simulations of the water dimer absorption spectrum

After the publication of the results of quantum-mechanical calculations of true bound water dimer spectral parameters by Schofield & Kjaergaard [52], the contribution of the dimer to the water vapour continuum began to be actively discussed. Ptashnik et al. [18] showed for the first time that the spectrum of true bound water dimer subbands (simulated using intensities and frequencies from quantum-mechanical calculations of Schofield & Kjaergaard [52] and equilibrium dimerization constants from Curtiss et al. [53]) explained particular pronounced absorption peaks in the observed near-IR in-band self-continuum spectra (see Fig. 1 in [18]). In the work of Daniel et al. [19] the role of water complexes (including H_2O-N_2, H_2O-O_2, and H_2O-Ar in water vapour mixture with atmospheric gases, in addition to the water dimer) in the formation of the continuum spectrum was discussed from a purely modelling perspective using the theoretical spectrum from [52]. A detailed consideration of this issue was presented by Ptashnik in [21], where a set of known experimental data for the water vapour continuum absorption in equilibrium conditions was used.

According to the bimolecular theory [16], true bound and quasibound H_2O dimers (henceforth b-dimers and q-dimers[2] respectively) determine the main component of pair states in water vapour volumes at close to atmospheric conditions, while the contribution of the so-called *free pairs* (defined as two H_2O monomers that experience one-off collisions and influence each other weakly [54]) is negligible. That is why the origin of the water vapour self-continuum absorption is usually considered mainly within the framework of the water dimer hypothesis [14,15,21]. A refined version of the water dimer model proposed in [22] explains the continuum by the combined contribution of b- and q-dimers

$$C_s(\nu,T) = K_{eq}^{b(fit)}(T)\sum_{\mathrm{i}} S_{\mathrm{i}}^{b}(T)\, f_{\mathrm{i}}^{b}(\Delta\nu_{\mathrm{i}},\gamma^{b}) + K_{eq}^{q(fit)}(T)\sum_{\mathrm{j}} S_{\mathrm{j}}^{q}(T) f_{\mathrm{j}}^{q}(\Delta\nu_{\mathrm{j}},\gamma^{q}), \quad (4)$$

[2] True bound dimer, for its formation from two H_2O molecules, requires a third-body collision; quasibound dimer relates to multiple-approach pair collisions resulting in the temporary stabilization of a pair which has total internal energy in excess of the dissociation threshold.

where C_s is the water vapour self-continuum cross-section [cm^2 $molec^{-1}$ atm^{-1}] (where 'atm' and 'molec' applies to the pressure and number of water monomers, respectively); S^b_i is intensity of i-th subband of b-dimers [cm $dimer^{-1}$]; S^q_i is intensity of i-th line of q-dimers [cm $dimer^{-1}$]; $f^b_i(\Delta\nu_i,\gamma^b)$ and $f^q_i(\Delta\nu_i,\gamma^q)$ are Voigt profiles [cm] with self-broadened halfwidths at half-maximum (HWHM) γ^b and γ^q [cm^{-1}] defined for b-dimer subbands and q-dimer lines, respectively; $\Delta\nu_i$ and $\Delta\nu_j$ are the distances from the centres of b-dimer subbands and q-dimer lines [cm^{-1}], respectively; $K^{b(fit)}_{eq}$ and $K^{q(fit)}_{eq}$ serve as fitting parameters of the model and have the meaning of the dimerization equilibrium constants K^b_{eq} and K^q_{eq} of b- and q-dimers (in [atm^{-1}] ≡ [$n_{dimers}n_{monomers}^{-1}$ per 1 atm of water monomers]), respectively:

$$K_{eq}^{b+q}(T) = K_{eq}^{b}(T) + K_{eq}^{q}(T), \quad (5)$$

where K^{b+q}_{eq} is a total equilibrium constant of water dimers. The introduction of fitting parameters was necessary due to the fact that the independent estimate of the dimerization equilibrium constant of q-dimers is still a challenging task. The ratio of b- and q-dimers as a function of temperature is considered in the framework of a statistical approach[55]. In turn, K^{b+q}_{eq} reflects the relationship between the partial pressure of water dimers, $P_{(H2O)2}$ and the total pressure of water vapour, P_{H2O}

$$K_{eq}^{b+q}(T) = \frac{P_{(H_2O)_2}}{P_{H_2O}^2}. \quad (6)$$

To date, estimates of the spectral parameters of water dimer transitions are available only for the true bound states (see below), while for the q-dimer such information is absent in the literature. Spectral properties of the latter are less pronounced compared to the true bound dimers, since quasibound dimers imply a fairly wide range of states that are between two extreme states of true bound dimer and free pair. Therefore, the direct calculation of the q-dimer spectrum is still particularly complex. In the water dimer model [22], it was suggested to use a simple approximation, according to which the q-dimer spectrum is calculated as a sum of strongly broadened H_2O monomer lines with doubled intensity S_i^{mon} (i.e. $S_i^q = 2\,S_i^{mon}$). Such an approach was chosen taking into account the characteristic short lifetime of quasibound states and from general considerations about the weak bond between two H_2O monomers forming q-dimers[56]. Obviously, the intensity of q-dimer lines can vary within certain limits relative to the doubled intensity of the H_2O monomer. However, a more universal and reasoned approximation has not yet been proposed.

3.1. Previous simulations

The water dimer model described above (Eq. (4)) was first applied for the in-band water vapour continuum in [22]. The results of *ab initio* calculations of b-dimer subbands' intensities and positions by Kjaergaard et al. (VPT2 [57]) and absolute intensity measurements by Kuyanov-Prozument et al. [58] were used to calculate b-dimer spectra. As a result, a good agreement of this model using two fitted parameters ($K^{b(fit)}_{eq}$ and $K^{q(fit)}_{eq}$) with experimental data [31] within absorption bands centred near 1600 and 3600 cm^{-1} was demonstrated.

The next important result in the development of the water dimer hypothesis was the refinement in estimation of the total dimerization constant $K^{b+q(estim)}_{eq}$ performed by Tretyakov et al. (2012)[59]. This estimate was then confirmed in the independent works by Ruscic(2013) [60] and Leforestier (2014) [61]. For b-dimer, two independent estimates of the equilibrium constant $K^{b(estim)}_{eq}$ are known from works of Scribano & Leforestier(2006) [62] and Buryak & Vigasin (2015) [63]. At present, the K^{b}_{eq} from [62] was multiplied by a factor of $\frac{e^{(D_0^{new}-D_0)}}{kT}$ to account for more accurate value of the dissociation energy D_0 = 1105 cm^{-1} from [64] instead of D_0 = 1234 cm^{-1} used in [62][3]. Taking into account the relationship between the total dimerization constant and b-dimer dimerization constant (Eq. (5)), the q-dimer dimerization constant $K^{q(estim)}_{eq}$ can be determined as the difference between $K^{b+q(estim)}_{eq}$ and $K^{b(estim)}_{eq}$.

Further, the water dimer model (Eq. (4)) was parameterized by fitting in the millimeter spectral region [65], within the rotational band [30,65], within the 1600 and 3600 cm^{-1} bands [32,33,65], and within the 8800 and 10 600 cm^{-1} absorption bands [34] (separately for each band). In all the studied vibrational-rotational bands, the model and experiment are in good spectral agreement (see the next Sect.). At the same time, the values of equilibrium constants $K^{b(fit)}_{eq}$ and $K^{q(fit.)}_{eq}$ derived from fitting of the model to experimental continuum spectra have demonstrated the overestimation of the total dimerization equilibrium constant $K^{b+q(fit)}_{eq}$ compared to the estimated values $K^{b+q(estim)}_{eq}$ across the whole considered temperature range from 268 to 431 K. In this subsection, the results of simulation of the continuum using the water dimer model, obtained by different scientific groups, are summarized. To avoid repetition, more detailed aspects of modeling the water dimer absorption spectra are considered in Subsect. 3.2.

Summarizing the considered results of simulations, the following conclusions were drawn.

First, the significant difference (up to several times) between the fitted and estimated equilibrium constants, $K^{b+q(fit)}_{eq}$ and $K^{b+q(estim)}_{eq}$ (see, for instance, Fig. 8 in [34]), can indicate only partial involvement of water dimers in forming in-band continuum spectrum. The calculations according to Eq. (4) using the independent estimates $K^{b(estim)}_{eq}$ and $K^{b+q(estim)}_{eq}$ instead of fitted parameters makes it possible to simulate more reliable water dimer absorption spectra, assuming good enough accuracy in the available spectroscopic information on the water dimers transitions. Such an approach allows the determination of the contribution of water dimers to the continuum absorption. This implies that the remaining value of the continuum is due to some other physical mechanism. For example, guided by this conclusion, Serov et al. [65] suggested a new model to describe the residual part (after subtraction of the water dimer contribution) of the continuum by contribution of the "non-Lorentzian" far wings of water monomer lines.

[3] D_0 plays an essential role in calculation of K^{b}_{eq}, as it contributes through the exponential term exp(D_0/kT) which is on the order of ~150 at room temperatures [62].

Secondly, it is worth noting the importance of the characteristic features of the b-dimer spectrum. Due to these spectral structure, the simultaneous fitting of the b- and q-dimer model spectra to the experimental continuum within each band has revealed that the fitted values of b-dimer equilibrium constant $K^{b(fit)}_{eq}$ are close to the known independent estimates $K^{b(estim.)}_{eq}$ [62,63]. In other words, the specific structure of b-dimer spectrum makes it possible to determine the b-dimer contribution to the continuum almost unambiguously, despite the involvement of other absorption mechanisms with a smoother structure (q-dimers, possible "non-Lorentzian" wings, or unknown others) in the continuum. Therefore, the observed difference between the fitted and estimated equilibrium constants, $K^{b+q(fit)}_{eq}$ and $K^{b+q(estim)}_{eq}$, should be explained mainly by the deviation of the fitted q-dimer equilibrium constant $K^{q(fit)}_{eq}$ from $K^{q(estim)}_{eq}$.

Thirdly, taking into account the markedly better spectral agreement of the experimental continuum with the water dimer model (Eq. (4)) using fitted parameters as compared to the widely used MT_CKD continuum model within the investigated IR absorption bands in a broad temperature range (from 268 to 431 K), it is possible to develop a semi-empirical modification of the in-band water dimer self-continuum model. The first steps in the development of such an in-band continuum model were made in our previous work [34] for 1600, 3600, 8800, and 10 600 cm^{-1} absorption bands. It was named the *dimer-based* continuum model. In this work, we propose an updated version based on the latest experimental continuum data for predicting the continuum absorption values within the extended spectral region from 50 to 11 200 cm^{-1}, excluding atmospheric windows, in a wide temperature range from 279to 431K.

3.2. Current simulations

Here, the water dimer model (Eq. (4)) was parameterized simultaneously within 150, 1600, 3600, 5300, 7200, 8800 and 10 600 cm^{-1}absorption bands. The experimental data on the water vapour self-continuum absorption are described in Sect. 2 (see Table 2).

Let us consider the first term on the right side of the Eq. (4). For the rotational absorption band, the results of *ab initio* calculations of b-dimer spectra are known from [57,66,67]. The most complete available b-dimer cross-sections from Scribano & Leforestier [66] were used here instead of the set of Voigt profiles and intensities in Eq. (4).These b-dimer cross-sections were fitted then to the experimental continuum spectra by varying the values of $K^{b(fit)}_{eq}$ parameter. Within the rovibrational absorption bands, obtaining information on individual spectral lines of b-dimer is a much more complicated task. In the literature, information on intensities and transition frequencies can be found only for the whole subbands, corresponding to vibrational transitions in water monomer units within b-dimer. Table 3 contains the spectroscopic information on b-dimer subband intensities and positions used in the present work to simulate b-dimer spectra within the rovibrational absorption subbands located in the spectral region from 1350 to 11 200 cm^{-1}. With this information, the b-dimer spectrum was simulated as a sum of b-dimer subbands using the Voigt profile and the *line-by-line* code [49].After completion of the main part of the work presented here, new data on the intensities and frequencies of true bound dimer transitions became available in [68,69] and [70] for spectral regions of H_2O monomer bands centred near 1600, 3600, 5300

and 7200 cm^{-1}. These works illustrate the many remaining challenges in estimating wavenumbers and intensities in *ab initio* calculations. However, there are no significant changes in these calculations compared to the previous ones that would markedly affect our current model[4]. These new data can be used in future work to update the new semi-empirical continuum model described in Sect. 5.

The HWHM of b-dimer subbands, γ^b, were determined individually for each band and at different temperatures to get better agreement between the model and experiment. They turned out to be nearly the same ~30 cm^{-1} (within experimental uncertainty) for the bands centered at 1600, 5300, 7200, 8800, and 10 600 cm^{-1} (so we set this value for all these bands), and ~19 cm^{-1} (instead of 17 cm^{-1} used in [32]) for the 3600 cm^{-1} band.

Table 3. Frequencies and intensities of b-dimer transitions within the IR bands*.

Local mode**	Wavenumber, cm^{-1}	Intensity, $cm^{-1}(dimer\ cm^{-2})^{-1}$	Source
	150 cm^{-1}		
–	50 – 572	cross-sections from [66]	[66]
	1600 cm^{-1}		
$\|00\rangle^+\|1\rangle$	1603.1	1.180E-17	[57]
$\|0\rangle_f\|0\rangle_b\|1\rangle$	1613.8	6.800E-18	[57]
–	1688.1	1.212E-23	Unpublished data from H.G. Kjaergaard (2008)
	1704.9	4.395E-19	
	1726.0	4.081E-19	
	1727.0	3.174E-19	
	1729.5	8.102E-19	
	1734.7	2.938E-20	
	1749.6	2.182E-19	
	1756.4	3.660E-19	
	1905.9	1.560E-18	
	1911.4	1.740E-19	
	3600 cm^{-1}		
$\|00\rangle^+\|2\rangle$	3163.0	1.240E-19	[57]
$\|0\rangle_f\|0\rangle_b\|2\rangle$	3200.0	4.320E-19	[71]
$\|0\rangle_f\|1\rangle_b\|0\rangle$	3616.0 (instead of 3597.4 in [58])	2.240E-17	[72]
$\|10\rangle^+\|0\rangle$	3655.8	7.720E-19	[58]
$\|1\rangle_f\|0\rangle_b\|0\rangle$	3721.0 (instead of 3730.1 in [58])	1.590E-17	[58]

[4] On average, the new intensity values differ by 15-20% randomly compared to the previous ones. However, direct comparison of intensity values does not provide a complete understanding of how exactly the simulated continuum value will change when new values of the transition intensities of true bound dimers are used. This is due to the fact that the halfwidth of the dimer subbands is the fitted parameter. Thus, a change in the halfwidth can compensate for the difference in the intensities of water dimers at individual frequencies.

$\|10\rangle^-\|0\rangle$	3745.0	7.300E-18	[58]
$\|1\rangle_f\|0\rangle_b\|0\rangle$	3890.4	1.100E-18	[71]
5300 cm^{-1}			
$\|0\rangle_f\|1\rangle_b\|1\rangle$	5219.0	5.600E-19	[57]
$\|10\rangle^+\|1\rangle$	5242.0	2.000E-20	[57]
$\|10\rangle^-\|1\rangle$	5329.0	5.82E-19	[73,74]***
$\|1\rangle_f\|0\rangle_b\|1\rangle$(82%)+$\|0\rangle_f\|1\rangle_b\|1\rangle$(13%)	5345.0	8.500E-19	[57]
7200 cm^{-1}			
$\|0\rangle_f\|1\rangle_b\|2\rangle$	6749.0	1.39E-21	[73,74]
$\|10\rangle^+\|2\rangle$	6789.0	1.08E-21	[73,74]
$\|10\rangle^-\|2\rangle$	6878.0	1.10E-20	[73,74]
$\|1\rangle_f\|0\rangle_b\|2\rangle$	6895.0	6.94E-21	[73,74]
$\|0\rangle_f\|2\rangle_b\|0\rangle$	7018.0	1.150E-19	[57]
$\|20\rangle^+\|0\rangle$(75 %)+$\|11\rangle^+\|0\rangle$(17 %)	7206.6	5.60E-20	[73,74]
$\|2\rangle_f\|0\rangle_b\|0\rangle$	7230.0	2.300E-19	[57]
$\|20\rangle^-\|0\rangle$	7245.0	2.46E-19	[73,74]
$\|1\rangle_f\|1\rangle_b\|0\rangle$(69 %)+$\|2\rangle_f\|0\rangle_b\|0\rangle$(25 %)	7362.0	1.64E-20	[73,74]
$\|11\rangle^+\|0\rangle$(78 %)+$\|20\rangle^+\|0\rangle$(18 %)	7449.0	1.30E-21	[73,74]
8800 cm^{-1}			
$\|0\rangle_f\|2\rangle_b\|1\rangle$	8530.5	7.39E-21	[73,74]
$\|20\rangle^+\|1\rangle$(70 %)+$\|11\rangle^+\|1\rangle$(16 %)	8754.9	2.69E-22	
$\|2\rangle_f\|0\rangle_b\|1\rangle$(63 %)+$\|1\rangle_f\|1\rangle_b\|1\rangle$(22 %)	8804.8	1.28E-20	
$\|20\rangle^-\|1\rangle$	8806.9	2.46E-20	
$\|1\rangle_f\|1\rangle_b\|1\rangle$(66 %)+$\|2\rangle_f\|0\rangle_b\|1\rangle$(25 %)	8930.1	4.03E-21	
$\|11\rangle^+\|1\rangle$(74 %)+$\|20\rangle^+\|1\rangle$(18 %)	9006.9	2.13E-24	
10 600 cm^{-1}			
$\|0\rangle_f\|2\rangle_b\|2\rangle$(69 %)+$\|0\rangle_f\|3\rangle_b\|0\rangle$(13 %)	10 057.5	3.14E-22	[73,74]
$\|0\rangle_f\|3\rangle_b\|0\rangle$(80 %)+$\|0\rangle_f\|2\rangle_b\|2\rangle$(12 %)	10 161.1	6.94E-22	
$\|30\rangle^+\|0\rangle$(77 %)+$\|21\rangle^+\|0\rangle$(9 %)	10 601	8.29E-22	
$\|3\rangle_f\|0\rangle_b\|0\rangle$(67 %)+$\|2\rangle_f\|1\rangle_b\|0\rangle$(12 %)	10 611	4.48E-21	
$\|30\rangle^-\|0\rangle$	10 615.3	8.06E-21	
$\|1\rangle_f\|2\rangle_b\|0\rangle$(68 %)+$\|3\rangle_f\|0\rangle_b\|0\rangle$(15 %)	10 673.7	6.05E-22	
$\|21\rangle^+\|0\rangle$(80 %)+$\|30\rangle^+\|0\rangle$(10 %)	10 869.7	3.58E-22	
$\|2\rangle_f\|1\rangle_b\|0\rangle$(74%)+$\|1\rangle_f\|2\rangle_b\|0\rangle$(15%)	10 889.1	8.51E-22	
$\|21\rangle^-\|0\rangle$	11 042	9.86E-22	

* The precision of the stated frequencies and intensities does not reflect their accuracy.

**According to the notation [57,73], $|x\rangle_f|y\rangle_b|z\rangle$ and $|xy\rangle_\pm|z\rangle$ label the vibrational modes in the donor and acceptor water unit, respectively. Here, *x* and *y* denote number of the vibrational quanta in the free ('f') and bound ('b') OH-stretching mode in the donor unit, respectively; *z* is the quantum in the HOH-bending mode; "±" refers to the symmetry of the stretching vibrations in the acceptor unit.

*** The intensities in [73,74] are given in the relative units so that the value of 100 was attributed to the strongest $|0\rangle_f|1\rangle_b|0\rangle$ transition. Here, the corresponding absolute values obtained using the intensity of the $|0\rangle_f|1\rangle_b|0\rangle$ band from [72] are presented.

Some modifications to the originally known parameters were made in this work as follows. The $|0\rangle_f|1\rangle_b|0\rangle$ and $|1\rangle_f|0\rangle_b|0\rangle$ b-dimer transitions were shifted from 3597.4 and 3730.1 cm^{-1}[58]to 3616.0 and 3721.0 cm^{-1}, respectively, based on the best agreement between the model water dimer spectra and the experimental continuum. The intensity of the strongest b-dimer transition ν_3 was set equal to $2.24\cdot10^{-17}$ cm dimer^{-1} [72] instead of $2.42\cdot10^{-17}$ cm dimer^{-1}[58], used for the same fitting of the water dimer model in [32]. In addition, the intensities of b-dimer subbands in the 5300, 7200, 8800, and 10 600 cm^{-1} bands, known from [73], were used according to the corrections made in [74]. Finally, in order to obtain absolute b-dimer transition

intensities from the relative values presented in [73,74], the absolute intensity of the strongest transition ν_3 from the work [72] was used and assumed to be 100.

The second term on the right side of the Eq. (4) corresponds to q-dimer cross-sections. These spectra were simulated as a sum of strongly broadened H_2O monomer lines with doubled intensities (as discussed above) using the Voigt profile and the *line-by-line* code [49]. The intensities and frequencies of H_2O monomer lines were taken from the HITRAN-2016 database [35] (the same version of the HITRAN used at the retrieval of the continuum).

Further, the simulated b- and q-dimer spectra were fitted to the experimental water vapour self-continuum using the least square method and two fitting parameters of the water dimer model: $K^{b(fit.)}_{eq}$ and $K^{q(fit.)}_{eq}$.

4. Discussion of the simulation results

The obtained γ^b value turned out have no temperature dependence within experimental uncertainty of the self-continuum spectra. Information on temperature dependences of the HWHM of b-dimer lines is not yet available. However, the obtained result is quite reasonable. Sinceb-dimer subbands consist of a huge number of strongly overlapped water dimer spectral lines, taking into account the temperature dependence of the HWHM of each dimer line will hardly lead to a noticeable change in γ^b value with temperature. Therefore, the HWHM of b-dimer subbands are considered as temperature independent. The values of b-dimer equilibrium constant $K^{b(fit)}_{eq}$ obtained from the fitting are discussed below.

The HWHM of q-dimer lines were set to γ^q=20 cm^{-1} for the rotational band and γ^q=10 cm^{-1} for the vibrational-rotational IR bands regardless of the temperature to get better agreement of the model with experimental spectra. The values are in a reasonable agreement with the estimate of average lifetime of q-dimer $\approx (2–5)\cdot10^{-12}$ s (or $\gamma \approx 7–20$ cm^{-1}), obtained from trajectory calculations for a pair of CO_2-Ar molecules [75] (despite the very different intermolecular interaction in this pair and in H_2O-H_2O).

The most significant and interesting results of the fitting is related to the obtained temperature dependence of b- and q-dimer equilibrium constants $K^{b(fit)}_{eq}$ and $K^{q(fit)}_{eq}$ (see Fig. 4). The region of lower available temperatures (≈ 280–300 K) should provide the most informative and reliable fitting results, because at these temperatures, the number of b- and q-dimers in water vapour should be approximately the same ($K^b_{eq} \sim K^q_{eq}$) [16] and spectral features of b-dimers are most pronounced. At higher temperatures, where q-dimers predominate ($K^b_{eq} < K^q_{eq}$), b-dimer equilibrium constant $K^{b(fit)}_{eq}$ would most likely be determined with less accuracy from the fitting. Besides, at lower temperatures (up to 300 K), there are experimental data on the water vapour self-continuum within the 3600 cm^{-1} absorption band. This spectral region is of special interest since it contains the two strongest transitions of b-dimer near 3616 cm^{-1} and 3721 cm^{-1} (see Table 3). As a result, the water dimer model within the 3600 cm^{-1} band should provide the most reliable fitting result, since b-dimer subbands provide the main contribution to the absorption here and their parameters are known from different independent calculations and experimental studies (see Table 3). Also, the fitting uncertainty caused by very approximate approach to simulation of q-dimer spectrum will be minimized due to the relatively small integrated contribution of q-dimers at lower temperatures.

The left panel of Fig. 4 contains information on fitted and estimated values of b-dimer equilibrium constants. Although the uncertainties of the fitted values of $K^{b(fit)}_{eq}$ goes beyond the area of estimates $K^{b(estim)}_{eq}$ [62,63] (between pink and black solid curves in left panel of Fig. 4), the absolute values of $K^{b(fit)}_{eq}$ in 1600, 3600, 5300 and 7200 cm^{-1} absorption bands are located near the average estimated value $<K^{b(estim)}_{eq}>$ (black dotted curve in left panel of Fig. 4). This result indicates that the water dimer model correctly takes into account the contribution of b-dimer to the water vapour continuum in these absorption bands, taking into consideration the structural and temperature features of b-dimer spectrum, despite the presence of at least the q-dimer contribution (and also the contribution of any additional absorption mechanism). In other absorption bands, the situation is different.

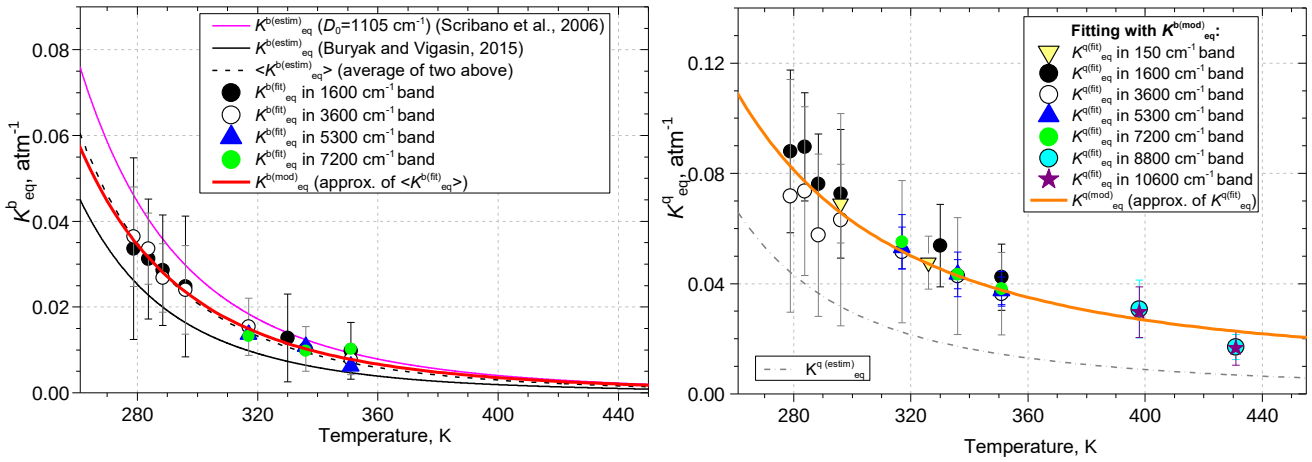

Fig. 4. Temperature dependences of b- and q-dimer equilibrium constants. Left panel: estimates of b-dimer equilibrium constant $K^{b(estim)}_{eq}$ from [62] (with corrected D_0 = 1105 cm^{-1}, pink solid curve) and [63] (black solid curve), and the average value $<K^{b(estim)}_{eq}>$ (black dotted curve); values of $K^{b(fit)}_{eq}$, obtained by fitting the water dimer model (Eq. (4)) to the experimental water vapour self-continuum spectra [26,31,32,34,47] (symbols); model b-dimer equilibrium constant $K^{b(mod)}_{eq}$, obtained by approximation of the fitted data $K^{b(fit)}_{eq}$ is shown by red solid curve. Right panel: estimate of q-dimer equilibrium constant $K^{q(estim)}_{eq}$, determined as a difference of $K^{b+q(estim)}_{eq}$ [59] and $<K^{b(estim)}_{eq}>$ [62,63] (grey dot-dash curve); values of $K^{q(fit)}_{eq}$, obtained by fitting the water dimer model (Eq. (4)) to the experimental water vapour self-continuum spectra [26,31,32,34,47] (symbols) using $K^{b(mod)}_{eq}$ from the left panel; model q-dimer equilibrium constant $K^{q(mod)}_{eq}$ obtained by approximation of the all fitted data $K^{q(fit)}_{eq}$ (orange solid curve).

In the rotational absorption band, the simultaneously fitted $K^{b(fit)}_{eq}$ and $K^{q(fit)}_{eq}$ values turned out to be very uncertain. This was caused by the fact that the b-dimer spectrum in this spectral region has a smooth featureless spectral structure, which, besides, is similar to the one for q-dimer. In the vibrational-rotational IR absorption bands, the intensive vibrational transitions of water monomer units within b-dimer cause the presence of well pronounced spectral peaks. These peaks are of special importance in determining the contribution of b-dimer to the water vapour self-continuum when the spectra of b- and q-dimers are jointly fitted to the experimental data. In the "near-visible" absorption bands (near 8800 and 10 600 cm^{-1}), uncertainties in the fitted $K^{b(fit)}_{eq}$ values also exceeded 100 %. This was caused by very weak contribution of b-dimers to the continuum at high temperatures. Due to this, the values of $K^{b(fit)}_{eq}$, in the 150 cm^{-1} and in two near-visible absorption bands were excluded from consideration. Only the $K^{b(fit)}_{eq}$ values obtained in 1600, 3600, 5300 and 7200 cm^{-1} absorption bands

were used when deriving $K^{b(mod)}_{eq}$ (red solid curve in the left panel of Fig. 4) by extrapolation of these values with an exponential function (see details in Sect. 5). Therefore, the final $K^{q(fit)}_{eq}$ values shown on the right panel of Fig. 4 were derived by fitting the water dimer model (Eq. (4)) to the experimental water vapour self-continuum with the equilibrium constants of b-dimer fixed at their $K^{b(mod)}_{eq}$ values (left panel of Fig. 4).

Based on the results of the analysis on temperature dependence of the b-dimer equilibrium constant, some conclusions can be made. One of the advantages of the model (Eq. (4)) [22,32] is that it makes it possible to identify the "real" contribution of b-dimer to the continuum absorption in the IR absorption bands near 1600, 3600, 5300 and 7200 cm^{-1}. This is achieved due to the fact that fitting the water dimer spectra to the experimental continuum allows verification of the estimated values of $K^{b(estim)}_{eq}$. Namely, the fitted values $K^{b(fit)}_{eq}$ turned out to be close to $K^{b(estim)}_{eq}$. It is important that this result was achieved despite using a very approximate approach to simulation of the q-dimer spectra.

At the same time, in all studied IR absorption bands, the values of $K^{q(fit)}_{eq}$ systematically exceed the estimated $K^{q(estim)}_{eq}$, obtained as a difference between the most reliable available estimates of the total equilibrium constant $K^{b+q(estim)}_{eq}$ [59–61] and $<K^{b(estim)}_{eq}>$ [62,63] (grey dot-dash curve in Fig. 4), by about 2-3.5 times over the temperature range from 280 to 430 K.

This result could be explained by two possibilities. According to the first one, an artificial overestimation of q-dimer equilibrium constant is found due to unaccounted transitions and underestimated transition intensities of the true bound dimers in the model. If this assumption is correct, then the use of more complete spectroscopic information, both for b- and q-dimers, would allow one to explain the experimental water vapour self-continuum only by H_2O dimers. Within the second possibility, the contribution of an additional absorption mechanism to the continuum may have a place (as already noted in Subsect. 3.1). A strong argument in favor of this assumption is that the much weaker temperature dependence of $K^{q(mod)}_{eq}(T)$ can be noted than for the estimation $K^{q(estim)}_{eq}(T)$ obtained by subtracting $<K^{b(estim)}_{eq}>$ [62,63] from $K^{b+q(estim)}_{eq}$ [59] (see orange solid and grey dot-dash curves in the right panel of Fig. 4). It is possible also that both described factors – possible significant uncertainties in spectroscopic information on b-dimer transitions (this can be partly verified by the use of the updated spectroscopic information from [68,70]) and an unaccounted absorption mechanism – may have place, which would complicate current attempts to describe the continuum absorption totally from a physical point of view.

Examples of the fitted water dimer model to the experimental continuum spectra using $K^{b(mod)}_{eq}$ and $K^{q(fit)}_{eq}$ in all studied absorption bands at different temperatures are presented in the left panels of Fig. 5. A quite detailed description of the spectral structure of the experimental continuum by this model is observed in most spectral regions, despite the use of the very approximate approach for simulating q-dimer spectrum.

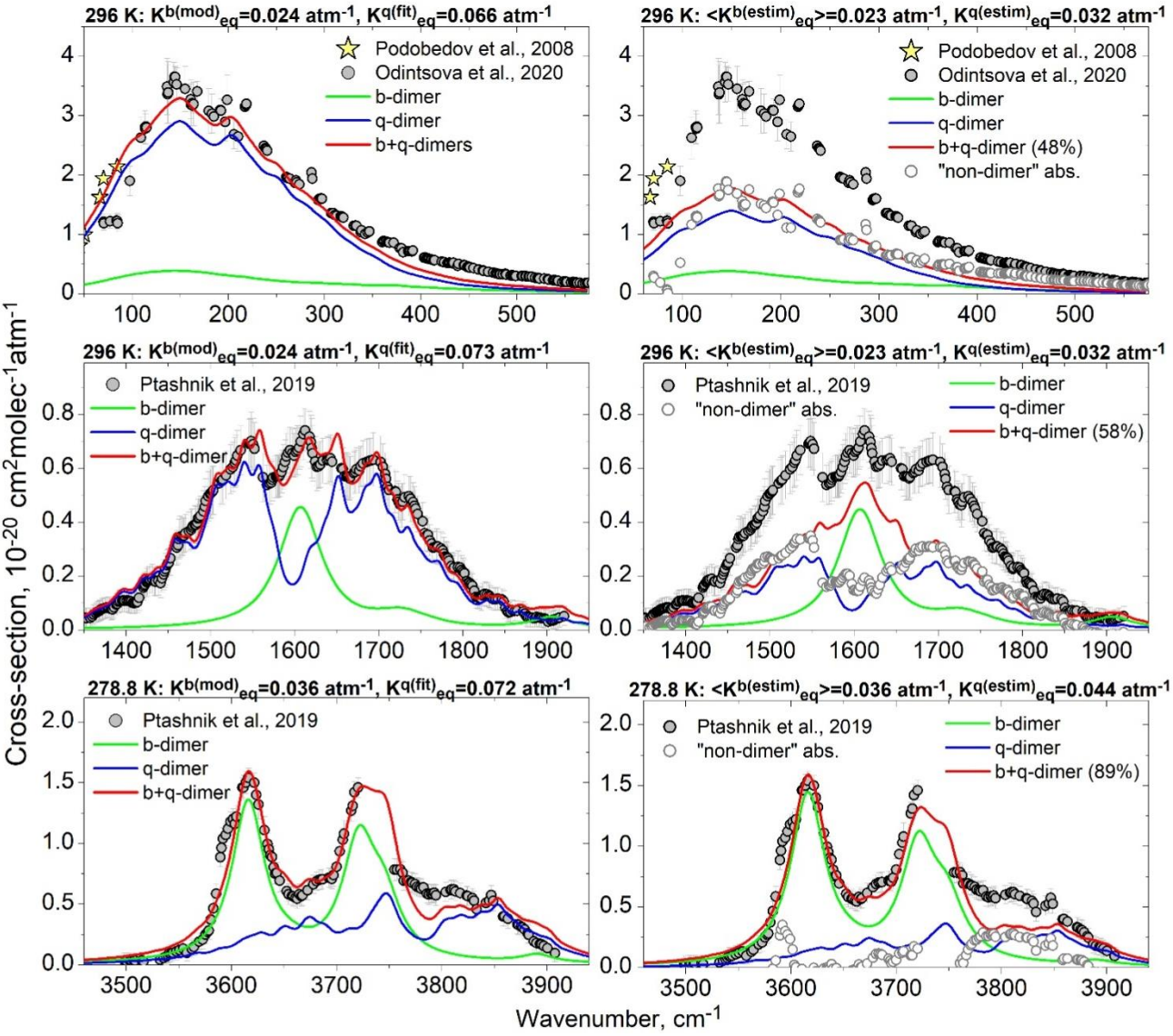

455 **Fig. 5.** Experimental water vapour self-continuum absorption (yellow stars and grey circles) and the results of the water dimer model parameterization (solid curves). Left panel: simulated absorption spectra of b-and q-dimers using $K^{b(mod)}_{eq}$ and $K^{q(fit)}_{eq}$, respectively (green and blue curves), and their joint spectrum (red curve). Right panel: simulated absorption spectra of b- and q-dimers using $\langle K^{b(estim)}_{eq}\rangle$ (average of the estimates of [62] (with D_0 = 1105 cm^{-1}) and [63]) and $K^{q(estim)}_{eq}$ (obtained as a difference of $K^{b+q(estim)}_{eq}$ [59] and $\langle K^{b(estim)}_{eq}\rangle$), respectively (green and blue curves), and their joint spectrum (red curve); "non-dimer" absorption (empty circles) obtained
460 as a difference between the experimental continuum and the total (b+q) dimer spectrum (red curve) simulated using independent estimates of the equilibrium constants $\langle K^{b(estim)}_{eq}\rangle$ and $K^{q(estim)}_{eq}$. Estimates of the integrated contribution of the absorption by water dimers to the continuum (in %) are given in parentheses.

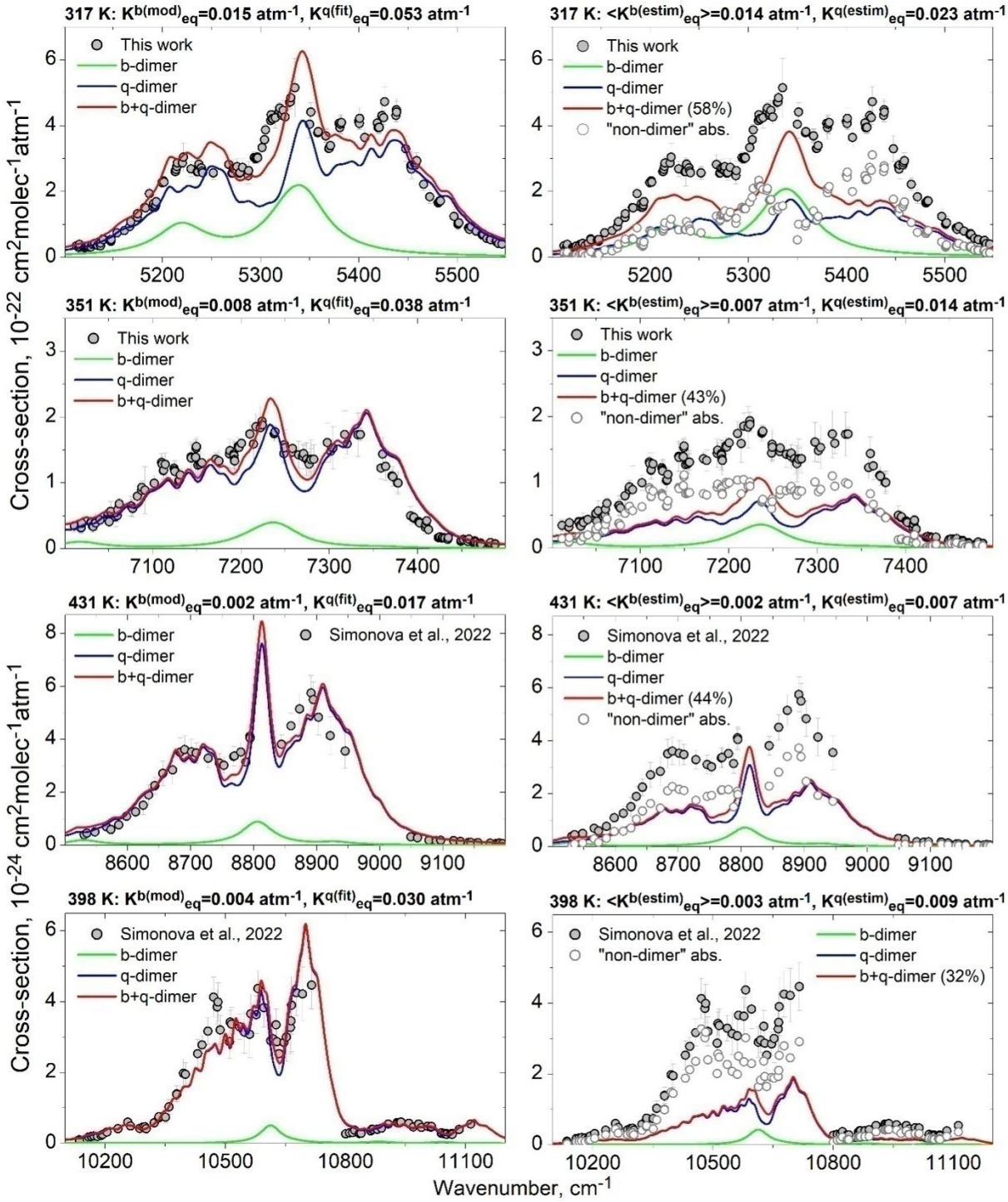

Fig. 5. Continued.

In the rotational absorption band, the water dimer model adequately reproduces the continuum in the spectral region from 50 to 280 cm^{-1}. It should be noted that in the low-frequency band wing, the model markedly exceeds the continuum obtained by Odintsova et al. [26]. However, the model is in excellent agreement with the experimental data from Podobedov et al. [39]. This result positively characterizes the tested water dimer model, since the data from Odintsova et al. [26] have indeed significant uncertainties in the spectral region from 70 to about 90 cm^{-1} caused by the sensitivity limits of the measuring setup. In the high-frequency wing of the rotational band (from 280 to 700 cm^{-1}), the model underestimates significantly the magnitude of the experimental continuum.

It should be noted that the model shows some pronounced spectral peaks that are absent in the experimental continuum. One of the examples is the peak at the centre of the 8800 cm^{-1} absorption band. It can be seen that there are no experimental data in this spectral interval, as well as in some other absorption bands in the regions near 3740, 5340, 8800 and 10 750 cm^{-1}. As a rule, strong absorption (the saturation effect) took place in such intervals, making the retrieval of the continuum impossible in these regions. Taking into account the fairly good agreement between the water dimer model and the experimental continuum in all studied absorption bands in a wide temperature range from 279 to 431 K, except for some cases (such as the high-frequency wing of the rotational absorption band extending far from the centre), it can be assumed that this model gives an adequate prediction of the continuum features but this cannot be confirmed due to the lack of experimental data.

The use of independent estimates for $<K^{b(estim)}_{eq}>$ (from [62] and [63]) and $K^{q(estim)}_{eq}$, obtained as a difference of $K^{b+q(estim)}_{eq}$ [59] and $<K^{b(estim)}_{eq}>$ in the model (Eq. (4)) (right panels of Fig. 5) made it possible to obtain an approximate estimate of the water dimer contribution to the experimental continuum absorption: from 40 % to 90 % (by the integrated absorption) with inverse temperature dependence in the interval from 279 to 431 K. The more accurate the available experimental continuum data and spectroscopic information on b- and q-dimer spectra are, the more reliable estimates of the water dimer contribution to the continuum can be obtained.

5. Semi-empirical dimer-based model of the water vapour self-continuum absorption

The results of this work provide a basis for development of a semi-empirical *dimer-based* continuum model. In particular, to modify the previous version of the water dimer model (Eq. (4)) [22,32], the model b- and q-dimer equilibrium constants, $K^{b(mod)}_{eq}$ and $K^{q(mod)}_{eq}$, have been introduced instead of the fitting parameters $K^{b(fit)}_{eq}$ and $K^{q(fit)}_{eq}$. This is because the model can be applied to all temperatures, whereas the fitting parameters are specific to measurements at a particular temperature. These new parameters gave the model an analytical form and made it possible to expand the spectral and temperature limits of application. As a result, the semi-empirical dimer-based continuum model reproduces the spectra of the in-band water vapour self-continuum within the extended spectral region from 50 to 11 200 cm^{-1} in a wide temperature range from 279 to 431 K. The updated model presents the in-band water vapour self-continuum absorption $C_s(\nu)$ [cm^2 $molec^{-1}$ atm^{-1}] at temperature T as the following:

$$C_s(\nu,T) = K_{eq}^{b(\mathrm{mod})}(T)\sum_i S_i^b(T)\, f_i^b(\Delta\nu_i,\gamma^b) + K_{eq}^{q(\mathrm{mod})}(T)\sum_j S_j^q(T) f_j^q(\Delta\nu_j,\gamma^q), \quad (7)$$

Where $K^{b(mod)}_{eq}$ and $K^{q(mod)}_{eq}$ are the model equilibrium constants of b- and q-dimers (in [atm^{-1}] ≡ [$n_{dimers}\, n_{monomers}^{-1}$ per 1 atm of water monomers]), respectively; S^b_i is the intensity of *i*-th subband of b-dimer [cm dimer^{-1}]; S^q_i is the intensity of *i*-th line of q-dimer [cm dimer^{-1}]; $f^b_i(\Delta\nu_i,\gamma^b)$ and $f^q_i(\Delta\nu_i,\gamma^q)$ are Voigt profiles [cm] with HWHM γ^b and γ^q [cm^{-1}] of b- and q-dimers, respectively; $\Delta\nu_i$ is the distance from the centres of b-dimer subbands; $\Delta\nu_j$ [cm^{-1}] is a distance from the q-dimer line centre.

The values of the model b- and q-dimer equilibrium constants, $K^{b(mod)}_{eq}$ and $K^{q(mod)}_{eq}$, are determined using the exponential temperature dependent function proposed earlier in [62]

$$K_{eq}^{b,q(\mathrm{mod})}(T) = a\cdot\exp\left(\frac{b}{T} + c\cdot T\right), \quad (8)$$

where T is temperature; a [atm^{-1}], b[K] and c [K^{-1}] are fixed parameters of the model, determined by approximation of $K^{b(fit)}_{eq}(T)$ values obtained in 1600, 3600, 5300 and 7200 cm^{-1} absorption bands (red solid curve in the left panel of Fig. 4), and the approximation of $K^{q(fit)}_{eq}$ values, obtained in all IR absorption bands studied here (orange solid curve in the right panel of Fig. 4), by the function from Eq. (8) (see values in Table 4). The values of other parameters in Eq. (7) remain the same as when fitting the previous version of the water dimer model from Eq. (4) to the experimental continuum (see Table 4).

Table 4. Parameters of the semi-empirical dimer-based continuum model.

Parameter	**Value**	
	b-dimer	**q-dimer**
$\boldsymbol{S_i}$, cm^{-1}(dimer cm^{-2})$^{-1}$	Data from the independent sources (Table 3).	$S_i^q = 2S_i^{mon}$, where the values of S_i^{mon} are from HITRAN-2016 database [35].
$\boldsymbol{\gamma}$, cm^{-1}	γ^b (in 1600, 5300, 7200, 8800 and 10 600 cm^{-1} bands) = 30 cm^{-1}; γ^b (in 3600 cm^{-1} band) = 19 cm^{-1}.	γ^q (in 150 cm^{-1} band) = 20 cm^{-1}; γ^q (in 1600, 3600, 5300,7200,8800 and 10 600 cm^{-1} bands) = 10 cm^{-1}.
Parameters for $K_{eq}^{b,q(mod)}$ from (Eq. (8)):		
$\boldsymbol{a}$, atm^{-1}	a^b = 4.7856·10^{-4} atm^{-1}	a^q = 4.7856·10^{-4} atm^{-1}
$\boldsymbol{b}$, K	b^b = 1580.7467 K	b^q = 1272.31769 K
$\boldsymbol{c}$, K^{-1}	c^b = -4.88·10^{-3} K^{-1}	c^q= 2.11·10^{-3} K^{-1}

Examples of the water vapour self-continuum spectra simulated using the new semi-empirical dimer-based model (Eq. (7–8)) within the studied IR bands at different temperatures are presented in Fig. 6 (all results can be found in the Supplementary material 2). Since the new model is aimed at reproducing the spectral features of the continuum, observed, as a rule, in the central part of the bands, in the rotational band it is limited to the spectral region from 50 to 280 cm^{-1}. After 300 cm^{-1} there are no spectral features and, as can be seen, the MT_CKD becomes more effective. Within the other absorption bands, it can be seen that the new model provides much better agreement with the experimental continuum compared to the

MT_CKD-3.5 model, especially if we take into account the wide temperature region considered here. This indicates the reliability of the dimer-based model in the studied spectral and temperature ranges. Therefore, the use of the semi-empirical dimer-based model seems to be more efficient for solving practical tasks that require taking into account the in-band water vapour self-continuum absorption. For example, the new model was shown to be superior to alternative approaches in removing the ambient air spectral features from Fourier-Transform near-IR spectra when investigating the spectra of liquid water [76]. With the advent of new experimental data in previously unexplored absorption bands at temperatures outside the range investigated here, it will be possible to extend the spectral and temperature boundaries of this model.

To summarize, the semi-empirical dimer-based continuum model has a set of important features. First, it provides a quite reliable prediction of spectral behaviour and magnitude of the in-band continuum in the wide spectral region from 50 to 11 200 cm^{-1} and temperature range from 279 to 431 K. This is confirmed by the obtained agreement of the model with 24 experimental water vapour self-continuum spectra. In particular, the average deviation from experiments near the centres of the absorption bands does not exceed 20 % for most studied data.

Finally, it is important to note that the semi-empirical dimer-based model includes a physically substantiated magnitude of b-dimer absorption, since the values of the introduced equilibrium constant lie within the theoretical estimates ($K^{b(estim)}_{eq}$ [63] $< K^{b(mod)}_{eq} \leq K^{b(estim)}_{eq}$ [62]), and the used spectroscopic parameters of b-dimer transitions are taken from independent sources (Table 3). Thus, further studies of the water quasibound dimer spectrum and other possible absorption mechanisms (one of which can be the “non-Lorentzian” wings of H_2O spectral lines) that presumably contribute to the continuum, will make it possible to develop a fully physically based model of the in-band water vapour continuum. Until then, the new semi-empirical model can be refined through the following steps: (1) update of the experimental continuum using the latest version of the HITRAN database (2020 version or more likely 2024); (2) simulation of water dimer spectra, using new spectroscopic information on transitions of the b-dimer [68,70], and their fitting to updated experimental continuum spectra with subsequent determination of the model effective dimerization constants. The planned upgrades do not take away from the merits and demonstrated effectiveness of the new continuum model and can be considered as a routine "technical" improvement.

Appendix B and the Supplementary material 1 contain all information needed for calculating the IR in-band water vapour self-continuum absorption spectra using the new semi-empirical dimer-based continuum model.

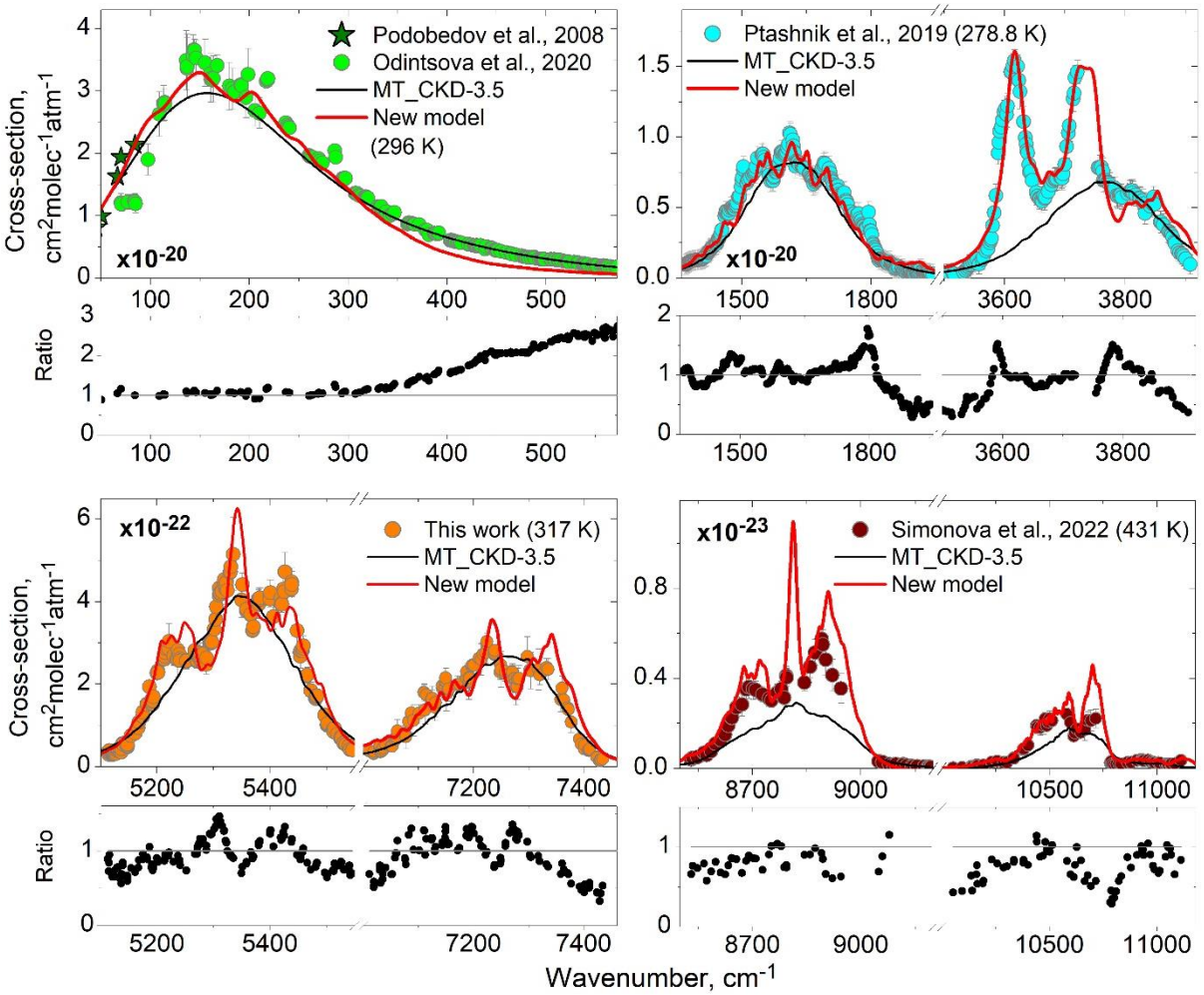

Fig.6. Water vapour self-continuum cross-sections within all investigated to date IR absorption bands: the examples of the experimental spectra (circles and stars), the MT_CKD-3.5 model (black curve) and the semi-empirical dimer-based model (red curve). Ratios of the experimental water vapour self-continuum spectra to the semi-empirical dimer-based model (empty circles). In the low-frequency wing of the rotational band (up to 100 cm^{-1}), the "ratio" spectrum was obtained using the experimental continuum data from Podobedov et al. [39].

6. Conclusions

The water vapour self-continuum absorption in the bands near 5300 and 7200 cm^{-1} has been newly retrieved from the experimental data of Paynter et al. (2009) [31] using the HITRAN-2016 database. This has allowed us to supplement a set of in-band experimental continuum spectra in the spectral region of 50–11 200 cm^{-1} by the up-to-date data. A joint consideration of the available experimental data on the continuum obtained with the FTS technique provides a more holistic understanding of the self-continuum absorption features. This has made it possible to use a unified approach to modeling the in-band continuum across almost the entire IR region and in a wide temperature range from 279 to 431 K.

The first results of large-scale parameterization of the continuum absorption with the model [22], carried out simultaneously in the strongest IR absorption bands (up to 11 200 cm^{-1}) in a wide temperature range, are presented. As a result, good spectral agreement between the model and measured continuum spectra was obtained. Introducing the model b- and q-dimer equilibrium constants, determined by approximation of the fitted $K^{b(fit)}_{eq}$ and $K^{q(fit)}_{eq}$ values, made it possible to construct a semi-empirical dimer-based continuum model. The model is easy to apply in radiative transfer codes and it noticeably outperforms the widely used MT_CKD continuum model in predicting the magnitude and spectral features of the in-band water vapour self-continuum in the temperature range of 279–431 K.

The highlighted differences between the total dimerization equilibrium constants obtained from the fitting and independent theoretical estimates – about 1.5–3 times with inverse temperature dependence at 279–431 K – make it possible to draw the following conclusions: 1) water dimers are responsible for at least 40–90 % of the in-band water continuum absorption, the proportion depending on absorption band and temperature within the 279–431 K range; 2) a more detailed study of the water dimer spectra (especially quasibound states) and other possible absorption mechanisms ("non-Lorentzian" wings of H_2O spectral lines and/or others) are needed before a fully physical representation of the continuum is possible. Further, using the obtained $K^{b(estim)}_{eq}$ and $K^{q(estim)}_{eq}$ values (Fig. 4), the respective "true bound+quasibound" dimer spectra (Fig. 5, right panels) can be subtracted from the current MT_CKD self-continuum values within bands to remove the pure water dimer contribution.

In summary, most radiative transfer codes used in climate and weather prediction models, and in remote sensing applications, use the MT_CKD model to represent the water vapour continuum. The MT_CKD model is largely based on laboratory observations over a limited number of wavenumbers and atmospheric conditions. Our work has exploited a wide range of pre-existing measurements to provide a much-refined model of self-continuum within the water vapour's absorption bands. The clear identification of the role of water dimers in this in-band continuum provides a much firmer understanding of the physical basis of the continuum, whilst at the same time identifying unresolved issues. The results of this study could be incorporated into future versions of MT_CKD and other continuum models, by separating dimer and non-dimer contributions to the in-band continuum; this would give greater confidence in its application for a broader range of conditions. In addition, the enhanced understanding of the self-continuum will allow more confident derivation of the in-band foreign continuum from measurements, as this depends heavily on the assumed strength of the self-continuum. Finally, the water vapour continuum is of most importance for the atmospheric energy balance in the windows between absorption bands; the clear attribution of the component of the in-band continuum to dimers offers promise for future improvements in understanding of the role of dimers in these windows.

Appendix A

Table A.1 Cross-section absorption of water vapour self-continuum, $C_s(\nu, T)$ [$cm^2 molec^{-1} atm^{-1}$] divided by 10^{-22}, retrieved from the experimental data (Paynter et al., 2009) using the HITRAN-2016 database, at 317, 336, and 351 K within 5300 and 7200 cm^{-1} absorption bands.

5300 cm^{-1}	317 K		336 K		351 K		7200 cm^{-1}	317 K		336 K		351 K	
ν, cm^{-1}	$C_s(\nu)$	$C^{err}_s(\nu)$	$C_s(\nu)$	$C^{err}_s(\nu)$	$C_s(\nu)$	$C^{err}_s(\nu)$	ν, cm^{-1}	$C_s(\nu)$	$C^{err}_s(\nu)$	$C_s(\nu)$	$C^{err}_s(\nu)$	$C_s(\nu)$	$C^{err}_s(\nu)$
5112.48	0.347	0.078	0.332	0.073	0.300	0.064	7011.46	0.382	0.112	0.299	0.088	0.347	0.089
5114.86	0.296	0.056	0.338	0.092	0.299	0.068	7019.12	0.315	0.068	0.312	0.089	0.315	0.085
5115.27	0.344	0.064	0.356	0.085	0.306	0.063	7019.28	0.325	0.077	0.322	0.090	0.320	0.080
5115.66	0.391	0.075	0.373	0.079	0.354	0.053	7019.98	0.366	0.112	0.369	0.094	0.386	0.059
5120.85	0.290	0.076	0.271	0.059	0.322	0.100	7030.36	0.469	0.119	0.397	0.082	0.405	0.059
5122.11	0.301	0.044	0.282	0.032	0.260	0.045	7030.46	0.490	0.095	0.405	0.092	0.399	0.065
5123.11	0.308	0.042	0.311	0.040	0.260	0.033	7030.54	0.506	0.078	0.411	0.099	0.394	0.074
5123.61	0.312	0.041	0.325	0.044	0.279	0.034	7031.97	0.358	0.105	0.325	0.096	0.344	0.091
5124.35	0.312	0.042	0.295	0.047	0.282	0.047	7032.99	0.366	0.119	0.354	0.116	0.335	0.097
5124.83	0.344	0.062	0.280	0.066	0.249	0.055	7035.36	0.397	0.139	0.423	0.157	0.408	0.129
5127.38	0.320	0.054	0.289	0.051	0.238	0.050	7035.77	0.444	0.093	0.448	0.122	0.392	0.068
5128.96	0.392	0.094	0.413	0.074	0.325	0.099	7040.77	0.539	0.189	0.461	0.110	0.436	0.080
5130.93	0.414	0.103	0.345	0.068	0.317	0.030	7049.43	--	--	0.487	0.107	0.513	0.082
5131.39	0.422	0.103	0.330	0.067	0.313	0.025	7049.82	--	--	0.488	0.107	0.530	0.052
5134.26	0.367	0.073	0.338	0.051	0.337	0.038	7050.98	0.498	0.142	0.455	0.106	0.408	0.080
5137.05	0.352	0.055	0.385	0.062	0.339	0.034	7052.50	0.496	0.150	0.460	0.123	0.565	0.152
5137.25	0.431	0.079	0.480	0.098	0.350	0.039	7058.03	0.650	0.174	0.483	0.186	0.485	0.154
5139.67	0.561	0.125	0.499	0.108	0.422	0.062	7059.95	0.708	0.135	0.524	0.146	0.502	0.093
5139.84	0.540	0.087	0.498	0.098	0.433	0.040	7060.58	0.712	0.070	0.610	0.089	0.591	0.069
5146.32	0.520	0.065	0.471	0.074	0.403	0.055	7062.39	0.868	0.277	0.756	0.140	0.681	0.084
5147.67	0.483	0.074	0.436	0.074	0.418	0.045	7075.57	0.809	0.174	0.566	0.185	0.649	0.148
5147.81	0.508	0.074	0.454	0.073	0.424	0.038	7076.16	0.792	0.199	0.557	0.187	0.647	0.090
5147.99	0.541	0.075	0.477	0.071	0.433	0.036	7077.45	0.725	0.295	0.545	0.191	0.609	0.125
5153.96	0.747	0.146	0.540	0.130	0.495	0.083	7077.48	0.727	0.294	0.547	0.191	0.615	0.128
5161.29	0.811	0.078	0.795	0.110	0.720	0.059	7082.86	1.095	0.083	0.870	0.222	0.795	0.152
5166.93	0.942	0.138	0.853	0.097	0.770	0.056	7087.55	1.289	0.097	--	--	0.887	0.090
5167.94	1.077	0.162	0.988	0.100	0.899	0.046	7087.89	1.302	0.099	1.051	0.144	0.930	0.097
5174.63	1.215	0.133	1.164	0.135	1.078	0.081	7091.30	1.125	0.383	0.869	0.302	0.889	0.358
5174.96	1.326	0.173	1.214	0.166	1.122	0.099	7101.83	1.297	0.212	1.103	0.104	0.994	0.117
5182.14	1.511	0.112	1.368	0.098	1.207	0.073	7110.36	1.803	0.179	1.463	0.144	1.311	0.133
5182.90	1.505	0.144	1.293	0.172	1.140	0.186	7110.73	1.797	0.208	1.435	0.179	1.285	0.109
5186.84	1.937	0.168	1.602	0.152	1.380	0.099	7112.30	1.374	0.338	1.238	0.263	1.184	0.134
5190.51	1.524	0.096	1.309	0.191	1.084	0.183	7112.35	--	--	1.234	0.264	1.191	0.135
5191.15	1.629	0.269	1.299	0.188	1.010	0.120	7114.50	1.743	0.152	1.596	0.308	1.282	0.170
5192.63	1.524	0.146	1.202	0.216	0.984	0.182	7124.47	1.634	0.139	1.379	0.104	1.221	0.070
5193.23	1.581	0.109	1.236	0.099	1.021	0.059	7124.99	1.660	0.205	1.357	0.224	1.195	0.130
5193.28	1.588	0.118	1.239	0.098	1.025	0.062	7125.30	1.650	0.305	--	--	1.173	0.175
5193.31	1.593	0.122	1.242	0.098	1.029	0.065	7129.69	1.452	0.254	1.149	0.250	1.027	0.161
5193.75	1.694	0.145	1.323	0.086	1.083	0.054	7130.43	1.439	0.327	1.188	0.238	1.042	0.118
5199.79	2.273	0.154	1.792	0.150	1.538	0.076	7131.30	1.555	0.134	1.238	0.158	1.119	0.095
5199.83	2.275	0.163	1.795	0.162	1.540	0.082	7143.59	1.899	0.164	1.518	0.226	1.396	0.225
5201.31	2.324	0.111	1.894	0.086	1.615	0.037	7143.80	1.965	0.252	1.601	0.359	1.379	0.212
5201.84	2.288	0.151	1.849	0.164	1.595	0.149	7148.55	1.938	0.312	--	--	1.391	0.266
5212.88	2.606	0.099	2.027	0.089	1.720	0.045	7148.90	1.903	0.140	1.500	0.328	1.390	0.264
5212.92	2.611	0.098	2.032	0.091	1.727	0.045	7149.39	2.067	0.199	1.687	0.184	1.528	0.128
5213.39	2.610	0.124	2.049	0.182	1.739	0.107	7149.64	2.158	0.228	1.747	0.197	1.551	0.130
5213.93	2.682	0.111	2.112	0.084	1.802	0.028	7151.40	1.780	0.426	1.468	0.297	1.268	0.222
5213.99	2.676	0.123	2.106	0.088	1.804	0.026	7153.57	1.803	0.218	1.466	0.303	1.281	0.237
5214.76	2.763	0.184	2.198	0.153	1.855	0.124	7155.03	1.875	0.209	1.494	0.202	1.303	0.178

5215.18	2.865	0.185	2.239	0.208	1.874	0.116	7155.63	1.886	0.190	--	--	1.308	0.128
5220.50	2.869	0.133	2.300	0.115	1.957	0.045	7171.65	1.986	0.217	1.573	0.132	1.361	0.095
5221.36	3.042	0.431	2.375	0.254	1.998	0.248	7175.10	1.995	0.190	1.538	0.245	1.332	0.161
5229.24	2.686	0.234	2.124	0.164	1.749	0.149	7187.09	2.157	0.329	1.670	0.198	1.443	0.218
5235.34	2.600	0.200	2.124	0.197	1.779	0.083	7187.50	2.308	0.099	1.724	0.180	1.488	0.116
5236.34	2.600	0.430	2.152	0.444	1.781	0.309	7191.68	2.039	0.258	1.655	0.349	1.439	0.212
5237.08	2.827	0.150	2.239	0.071	1.906	0.047	7192.08	2.076	0.447	1.556	0.472	1.415	0.219
5239.79	2.721	0.181	2.250	0.116	1.916	0.197	7192.72	2.164	0.210	1.604	0.275	1.356	0.241
5240.34	2.619	0.143	2.110	0.187	1.827	0.092	7192.97	2.148	0.313	1.563	0.264	1.334	0.157
5241.10	2.571	0.119	2.065	0.100	1.759	0.105	7197.12	2.442	0.154	1.818	0.198	1.555	0.129
5251.79	2.558	0.196	2.064	0.109	1.693	0.073	7197.82	2.467	0.109	1.816	0.103	1.538	0.057
5251.93	2.568	0.173	2.055	0.124	1.687	0.077	7200.60	2.458	0.070	1.920	0.170	1.600	0.032
5267.52	2.821	0.297	2.163	0.173	1.755	0.086	7210.19	2.633	0.137	2.003	0.272	1.744	0.180
5270.91	2.551	0.129	1.963	0.133	1.587	0.112	7214.19	2.604	0.381	1.888	0.384	1.590	0.287
5271.70	2.572	0.074	1.985	0.116	1.624	0.032	7217.09	2.725	0.257	2.174	0.232	1.853	0.201
5272.12	2.694	0.278	2.004	0.260	1.625	0.132	7222.04	2.757	0.237	2.113	0.319	1.841	0.316
5273.63	2.677	0.195	2.104	0.131	1.740	0.107	7223.90	2.983	0.108	2.268	0.259	1.936	0.131
5275.03	2.640	0.152	2.082	0.187	1.744	0.149	7224.23	3.030	0.195	2.258	0.179	1.882	0.113
5275.46	2.637	0.165	2.058	0.103	1.706	0.050	7237.64	2.727	0.130	2.095	0.177	1.746	0.120
5275.77	2.653	0.149	2.061	0.079	1.720	0.044	7238.01	2.751	0.166	2.057	0.109	1.759	0.108
5276.08	2.754	0.238	2.111	0.099	1.761	0.036	7238.59	2.820	0.108	2.088	0.125	1.778	0.070
5276.11	2.752	0.244	2.113	0.104	1.764	0.036	7248.70	2.290	0.176	1.733	0.219	1.443	0.142
5278.27	2.557	0.136	1.948	0.126	1.584	0.069	7249.16	2.475	0.247	1.837	0.379	1.577	0.229
5278.99	2.578	0.233	1.930	0.260	1.540	0.186	7249.43	2.358	0.437	1.756	0.394	1.533	0.207
5281.55	2.734	0.259	2.107	0.342	1.730	0.269	7257.95	2.246	0.177	1.718	0.145	1.466	0.110
5287.26	2.480	0.247	1.864	0.221	1.463	0.192	7258.34	2.307	0.083	1.770	0.112	1.525	0.049
5287.71	2.635	0.285	1.895	0.172	1.493	0.105	7265.37	2.252	0.382	1.689	0.379	1.428	0.203
5293.60	3.028	0.176	2.217	0.087	1.784	0.046	7269.68	2.181	0.240	1.657	0.136	1.409	0.092
5295.08	2.994	0.074	2.250	0.078	1.834	0.061	7270.39	2.142	0.354	1.594	0.334	1.398	0.188
5295.43	3.025	0.080	2.292	0.111	1.875	0.105	7270.86	2.293	0.159	1.705	0.176	1.445	0.121
5296.18	3.019	0.167	2.293	0.076	1.880	0.061	7274.31	2.138	0.260	1.594	0.450	1.360	0.247
5296.78	3.045	0.125	2.326	0.122	1.903	0.113	7276.54	2.048	0.162	1.504	0.490	1.306	0.163
5297.07	3.024	0.145	2.316	0.134	1.899	0.077	7277.22	1.941	0.447	1.477	0.502	1.285	0.274
5301.60	3.338	0.137	2.416	0.101	1.953	0.050	7279.01	1.935	0.312	1.580	0.554	1.359	0.300
5304.15	3.576	0.141	2.733	0.200	2.186	0.192	7279.52	2.133	0.256	1.573	0.217	1.350	0.172
5304.99	3.875	0.162	2.798	0.135	2.243	0.079	7282.32	2.142	0.319	1.631	0.316	1.360	0.216
5310.27	4.155	0.104	2.944	0.104	2.333	0.073	7297.77	2.675	0.473	1.970	0.481	1.611	0.298
5310.66	4.330	0.101	3.014	0.104	2.375	0.064	7301.70	2.334	0.083	1.713	0.153	1.481	0.175
5311.85	4.199	0.098	3.048	0.141	2.442	0.110	7304.14	2.326	0.439	1.745	0.377	1.529	0.321
5312.29	4.221	0.151	3.014	0.098	2.399	0.078	7317.40	2.356	0.500	1.994	0.597	1.734	0.360
5312.32	4.220	0.149	3.014	0.101	2.397	0.086	7320.21	2.227	0.244	1.769	0.251	1.594	0.158
5312.38	4.217	0.146	3.009	0.115	2.389	0.105	7332.48	2.404	0.216	1.926	0.458	1.733	0.332
5312.42	4.205	0.155	2.994	0.147	2.378	0.125	7335.24	2.361	0.257	1.939	0.144	1.737	0.096
5314.98	4.245	0.321	3.081	0.491	2.404	0.274	7358.36	1.626	0.291	1.288	0.221	1.225	0.166
5319.10	4.454	0.129	3.168	0.093	2.518	0.048	7360.32	1.899	0.299	1.584	0.336	1.437	0.253
5319.47	4.537	0.160	3.186	0.098	2.512	0.111	7363.76	1.622	0.302	1.341	0.204	1.252	0.213
5321.42	4.320	0.095	3.075	0.137	2.432	0.094	7370.90	1.429	0.162	1.211	0.183	1.108	0.092
5321.96	4.370	0.158	3.095	0.123	2.467	0.055	7371.82	1.386	0.143	1.148	0.150	1.095	0.147
5323.12	4.470	0.293	3.093	0.195	2.439	0.085	7377.24	1.082	0.251	1.086	0.182	0.999	0.164
5324.91	4.270	0.222	2.985	0.178	2.343	0.186	7377.45	--	--	1.083	0.184	1.001	0.171
5329.46	4.708	0.155	3.299	0.150	2.527	0.144	7377.80	--	--	1.077	0.186	0.996	0.131
5330.35	4.725	0.218	3.319	0.363	2.586	0.260	7391.97	0.668	0.134	0.508	0.137	0.500	0.140
5330.80	4.848	0.161	3.313	0.308	2.553	0.342	7395.36	0.551	0.158	--	--	0.465	0.060
5334.99	5.155	0.889	3.522	0.721	2.721	0.678	7395.64	0.545	0.155	--	--	0.478	0.092
5349.91	4.041	0.426	2.940	0.198	2.253	0.251	7400.88	0.435	0.076	0.427	0.097	0.412	0.061
5351.28	4.419	0.278	3.249	0.291	2.650	0.272	7401.54	0.525	0.187	0.410	0.123	0.407	0.055
5358.18	3.783	0.122	2.965	0.128	2.465	0.089	7402.29	--	--	0.403	0.118	0.393	0.048
5358.69	3.823	0.097	2.980	0.170	2.499	0.078	7408.50	0.397	0.095	0.340	0.075	0.325	0.102
5358.72	3.822	0.102	2.976	0.172	2.500	0.081	7409.13	0.386	0.086	0.335	0.073	0.366	0.052

5366.33	3.684	0.229	2.862	0.185	2.353	0.134	7409.17	0.387	0.086	0.335	0.075	0.368	0.052
5366.37	3.692	0.207	2.862	0.177	2.353	0.129	7409.89	0.411	0.090	0.353	0.120	0.412	0.092
5366.40	3.697	0.192	2.862	0.171	2.352	0.128	7410.31	0.426	0.092	0.380	0.091	0.426	0.059
5369.45	3.303	0.100	2.573	0.082	2.107	0.048	7412.21	--	--	0.358	0.081	0.291	0.076
5369.85	3.312	0.110	2.554	0.064	2.136	0.035	7423.30	0.231	0.077	0.180	0.064	0.168	0.053
5371.09	3.387	0.138	2.614	0.157	2.164	0.098	7423.82	0.221	0.073	0.195	0.061	0.170	0.048
5371.12	3.395	0.116	2.615	0.150	2.166	0.092	7424.22	--	--	0.205	0.060	0.169	0.036
5379.84	4.072	0.214	3.014	0.209	2.504	0.128	7425.21	--	--	0.231	0.055	0.180	0.048
5380.67	3.942	0.349	3.059	0.458	2.522	0.355	7427.46	--	--	0.184	0.045	0.159	0.039
5381.26	4.046	0.289	3.145	0.212	2.601	0.232	7428.69	0.137	0.035	0.158	0.040	0.170	0.041
5381.29	4.052	0.276	3.149	0.199	2.607	0.212	7430.63	0.168	0.043	0.151	0.039	0.163	0.055
5382.33	4.096	0.237	3.064	0.157	2.584	0.155	7430.69	0.169	0.043	0.151	0.039	0.160	0.055
5399.82	4.134	0.147	3.275	0.120	2.760	0.080	7434.08	0.187	0.077	0.138	0.038	0.142	0.050
5400.23	4.118	0.138	3.259	0.120	2.775	0.090	7434.66	--	--	0.179	0.047	0.169	0.046
5400.53	4.066	0.187	3.260	0.144	2.775	0.059	7448.83	--	--	0.121	0.031	0.112	0.018
5400.81	4.220	0.311	3.338	0.137	2.829	0.086	7449.39	--	--	0.119	0.042	0.130	0.030
5406.06	3.642	0.295	2.881	0.255	2.399	0.203	7451.65	--	--	0.141	0.049	0.140	0.048
5418.73	4.082	0.180	3.281	0.127	2.799	0.079	7451.73	--	--	0.142	0.050	0.136	0.048
5419.60	3.939	0.188	3.192	0.168	2.728	0.058	7455.84	--	--	0.126	0.035	0.138	0.028
5420.73	3.957	0.156	3.181	0.145	2.735	0.066	7456.79	--	--	0.127	0.042	0.108	0.025
5420.81	3.945	0.168	3.165	0.162	2.725	0.064	7457.89	--	--	0.120	0.027	0.145	0.035
5423.52	4.306	0.335	3.503	0.293	2.985	0.380	7463.78	--	--	0.110	0.038	0.080	0.023
5425.27	4.247	0.208	3.478	0.115	2.988	0.093	7463.90	--	--	0.114	0.040	0.087	0.018
5426.16	4.730	0.464	3.666	0.405	3.110	0.294	7464.01	--	--	0.117	0.039	0.092	0.015
5437.67	4.313	0.188	3.519	0.192	3.064	0.104	7464.56	--	--	0.122	0.027	0.118	0.032
5438.19	4.485	0.330	3.639	0.383	3.136	0.243	7464.79	--	--	0.105	0.025	0.106	0.032
5438.43	4.414	0.321	3.602	0.337	3.102	0.195	7465.11	--	--	0.104	0.026	0.102	0.027
5447.81	3.302	0.389	2.672	0.321	2.324	0.252	7468.00	--	--	0.100	0.027	0.067	0.021
5452.88	2.784	0.180	2.329	0.141	2.043	0.082	7470.85	--	--	0.088	0.021	0.062	0.022
5453.03	2.766	0.206	2.330	0.143	2.035	0.083	7471.15	--	--	0.087	0.020	0.086	0.026
5453.41	2.682	0.131	2.262	0.083	2.009	0.044	7471.79	--	--	0.086	0.020	0.069	0.020
5454.07	2.809	0.422	2.331	0.363	2.018	0.230	7480.79	--	--	0.084	0.020	0.069	0.016
5457.49	2.809	0.237	2.472	0.299	2.201	0.157	7481.03	--	--	0.086	0.021	0.070	0.017
5458.08	2.873	0.200	2.538	0.134	2.230	0.127	7481.23	--	--	0.087	0.021	0.078	0.017
5458.85	2.936	0.241	2.518	0.122	2.244	0.161	7482.24	--	--	0.094	0.024	0.095	0.026
5465.84	2.219	0.187	1.809	0.112	1.600	0.044	7487.30	--	--	0.105	0.023	0.070	0.020
5472.06	1.843	0.208	1.619	0.213	1.408	0.113	7487.52	--	--	0.106	0.023	0.074	0.020
5480.57	1.660	0.141	1.449	0.107	1.283	0.071	7487.64	--	--	0.105	0.023	0.068	0.017
5480.95	1.651	0.078	1.450	0.051	1.292	0.046	--	--	--	--	--	--	--
5481.92	1.682	0.119	1.520	0.132	1.361	0.081	--	--	--	--	--	--	--
5482.47	1.721	0.084	1.476	0.105	1.363	0.080	--	--	--	--	--	--	--
5483.02	1.709	0.084	1.530	0.097	1.384	0.038	--	--	--	--	--	--	--
5483.11	1.712	0.074	1.540	0.079	1.391	0.036	--	--	--	--	--	--	--
5496.77	1.245	0.207	1.027	0.157	0.980	0.179	--	--	--	--	--	--	--
5500.88	1.006	0.120	0.933	0.125	0.837	0.100	--	--	--	--	--	--	--
5501.23	1.033	0.194	0.939	0.155	0.859	0.097	--	--	--	--	--	--	--
5501.83	1.051	0.195	0.984	0.211	0.880	0.175	--	--	--	--	--	--	--
5511.55	0.891	0.134	0.788	0.084	0.716	0.025	--	--	--	--	--	--	--
5512.20	0.881	0.139	0.777	0.113	0.707	0.080	--	--	--	--	--	--	--
5512.26	0.879	0.140	0.788	0.116	0.710	0.076	--	--	--	--	--	--	--
5512.58	0.853	0.130	0.806	0.101	0.725	0.053	--	--	--	--	--	--	--
5514.43	0.930	0.075	0.794	0.131	0.688	0.114	--	--	--	--	--	--	--
5519.55	0.794	0.122	0.735	0.093	0.719	0.086	--	--	--	--	--	--	--
5519.58	0.795	0.122	0.739	0.108	0.722	0.093	--	--	--	--	--	--	--
5525.46	0.688	0.149	0.665	0.118	0.604	0.058	--	--	--	--	--	--	--
5525.52	0.699	0.147	0.668	0.115	0.605	0.056	--	--	--	--	--	--	--
5525.58	0.711	0.146	0.656	0.113	0.605	0.056	--	--	--	--	--	--	--
5525.97	0.719	0.140	0.677	0.166	0.582	0.073	--	--	--	--	--	--	--
5526.62	0.701	0.133	0.723	0.115	0.665	0.069	--	--	--	--	--	--	--

5526.66	0.700	0.132	0.726	0.109	0.667	0.069	--	--	--	--	--	--	--
5526.75	0.697	0.131	0.731	0.097	0.673	0.062	--	--	--	--	--	--	--
5530.34	0.576	0.090	0.601	0.075	0.572	0.039	--	--	--	--	--	--	--
5530.38	0.571	0.089	0.605	0.079	0.576	0.042	--	--	--	--	--	--	--
5533.76	0.543	0.083	0.649	0.116	0.518	0.075	--	--	--	--	--	--	--
5534.26	0.539	0.082	0.525	0.090	0.432	0.048	--	--	--	--	--	--	--
5539.80	0.488	0.079	0.442	0.078	0.381	0.040	--	--	--	--	--	--	--
5539.85	0.485	0.082	0.439	0.080	0.378	0.041	--	--	--	--	--	--	--
5540.09	0.473	0.096	0.427	0.094	0.365	0.047	--	--	--	--	--	--	--
5540.40	0.515	0.120	0.418	0.092	0.329	0.082	--	--	--	--	--	--	--
5542.27	0.413	0.084	0.371	0.067	0.363	0.052	--	--	--	--	--	--	--
5542.30	0.418	0.082	0.370	0.066	0.364	0.051	--	--	--	--	--	--	--
5545.68	0.404	0.077	0.366	0.061	0.338	0.054	--	--	--	--	--	--	--
5558.39	--	--	0.164	0.029	0.152	0.026	--	--	--	--	--	--	--
5558.63	--	--	0.194	0.036	0.172	0.031	--	--	--	--	--	--	--
5558.89	--	--	0.229	0.040	0.200	0.040	--	--	--	--	--	--	--
5559.24	--	--	0.227	0.045	0.201	0.026	--	--	--	--	--	--	--
5559.27	--	--	0.227	0.046	0.201	0.026	--	--	--	--	--	--	--
5559.54	--	--	0.226	0.049	0.192	0.019	--	--	--	--	--	--	--
5559.60	--	--	0.225	0.048	0.192	0.018	--	--	--	--	--	--	--
5559.64	--	--	0.224	0.047	0.191	0.019	--	--	--	--	--	--	--
5559.72	--	--	0.223	0.046	0.190	0.021	--	--	--	--	--	--	--
5559.78	--	--	0.223	0.044	0.189	0.021	--	--	--	--	--	--	--
5559.93	--	--	0.224	0.044	0.191	0.020	--	--	--	--	--	--	--
5562.28	--	--	0.204	0.052	0.198	0.045	--	--	--	--	--	--	--
5562.35	--	--	0.202	0.051	0.200	0.046	--	--	--	--	--	--	--
5563.45	--	--	0.185	0.042	0.184	0.043	--	--	--	--	--	--	--
5568.52	--	--	0.156	0.033	0.175	0.037	--	--	--	--	--	--	--
5568.86	--	--	0.188	0.044	0.177	0.036	--	--	--	--	--	--	--
5571.32	--	--	0.194	0.040	0.167	0.034	--	--	--	--	--	--	--
5571.94	--	--	0.197	0.037	0.183	0.041	--	--	--	--	--	--	--
5572.24	--	--	0.184	0.036	0.175	0.031	--	--	--	--	--	--	--
5572.72	--	--	0.163	0.035	0.143	0.022	--	--	--	--	--	--	--
5576.71	--	--	0.125	0.023	0.120	0.028	--	--	--	--	--	--	--
5576.82	--	--	0.124	0.023	0.124	0.024	--	--	--	--	--	--	--
5576.85	--	--	0.123	0.023	0.125	0.022	--	--	--	--	--	--	--
5576.91	--	--	0.123	0.023	0.127	0.020	--	--	--	--	--	--	--
5581.31	--	--	0.202	0.040	0.167	0.047	--	--	--	--	--	--	--
5584.50	--	--	0.154	0.029	0.127	0.028	--	--	--	--	--	--	--
5586.99	--	--	0.150	0.027	0.127	0.024	--	--	--	--	--	--	--
5587.06	--	--	0.147	0.027	0.128	0.024	--	--	--	--	--	--	--
5587.09	--	--	0.146	0.027	0.128	0.024	--	--	--	--	--	--	--
5587.18	--	--	0.143	0.026	0.128	0.026	--	--	--	--	--	--	--
5587.29	--	--	0.139	0.026	0.127	0.028	--	--	--	--	--	--	--
5587.35	--	--	0.137	0.026	0.121	0.024	--	--	--	--	--	--	--
5587.59	--	--	0.128	0.023	0.124	0.019	--	--	--	--	--	--	--
5587.63	--	--	0.131	0.023	0.125	0.019	--	--	--	--	--	--	--
5587.77	--	--	0.142	0.021	0.136	0.022	--	--	--	--	--	--	--
5587.88	--	--	0.149	0.021	0.145	0.023	--	--	--	--	--	--	--
5587.94	--	--	0.150	0.024	0.148	0.023	--	--	--	--	--	--	--
5588.01	--	--	0.152	0.028	0.149	0.023	--	--	--	--	--	--	--
5588.13	--	--	0.155	0.034	0.151	0.021	--	--	--	--	--	--	--
5588.18	--	--	0.155	0.034	0.149	0.020	--	--	--	--	--	--	--
5588.31	--	--	0.154	0.035	0.143	0.018	--	--	--	--	--	--	--
5588.37	--	--	0.153	0.035	0.141	0.016	--	--	--	--	--	--	--
5588.42	--	--	0.153	0.035	0.139	0.015	--	--	--	--	--	--	--
5588.45	--	--	0.153	0.035	0.137	0.014	--	--	--	--	--	--	--
5588.48	--	--	0.153	0.035	0.136	0.014	--	--	--	--	--	--	--
5588.60	--	--	0.152	0.035	0.131	0.013	--	--	--	--	--	--	--

5588.64	--	--	0.151	0.035	0.129	0.013	--	--	--	--	--	--	--
5589.02	--	--	0.149	0.029	0.130	0.016	--	--	--	--	--	--	--
5589.08	--	--	0.148	0.028	0.129	0.016	--	--	--	--	--	--	--
5589.13	--	--	0.148	0.028	0.129	0.016	--	--	--	--	--	--	--
5591.37	--	--	0.154	0.029	0.102	0.014	--	--	--	--	--	--	--

Appendix B

Here the information for calculating the IR in-band water vapour self-continuum absorption spectra using the new semi-empirical dimer-based continuum model is presented. The continuum is calculated by the following expressions and tabular data presented in the Supplementary material 1:

$$C_s(\nu,T) = K_{eq}^{b(\mathrm{mod})}(T)C_0^b(\nu) + K_{eq}^{q(\mathrm{mod})}(T)C_0^q(\nu,T), \quad \text{(B.1)}$$

where $C_s(\nu,T)$ is the model water vapour self-continuum cross-sections [cm^{2}molec^{-1}atm^{-1}]; $C_0^b(\nu)$ and $C_0^q(\nu,T)$ are the model pressure independent cross-sections of b- and q-dimers, respectively, [cm^{2}molec^{-1}] (see data in the Supplementary material 1); $K^{b(\mathrm{mod})}_{eq}$ and $K^{q(\mathrm{mod})}_{eq}$ are the model (effective) equilibrium constants of b- and q-dimers [atm^{-1}], respectively, defined as

$$K_{eq}^{b(\mathrm{mod})}(T) = 4.7856 \cdot 10^{-4} \cdot \exp\left(\frac{1580.7467}{T} - 4.88 \cdot 10^{-3} \cdot T\right), \quad \text{(B.2)}$$

$$K_{eq}^{q(\mathrm{mod})}(T) = 4.7856 \cdot 10^{-4} \cdot \exp\left(\frac{1272.31769}{T} + 2.11 \cdot 10^{-3} \cdot T\right). \quad \text{(B.3)}$$

The presented data are suitable for calculating the continuum at 279–431K in the IR absorption bands located within 50–11200 cm^{-1} spectral region.

Also, for some applications, it can be useful to have information not about the *model* (effective) cross-sections of the dimers (left panel of Fig.5), but about the "real" contribution of b- and q-dimers within bands (right panels of Fig. 5). The most reliable current information about cross-section of water dimers ($C_d(\nu,T)$) suggested in our work can be obtained from similar to B.1-B.3 equation:

$$C_d(\nu,T) = K_{eq}^{b(\mathrm{estim})}(T)C_0^b(\nu) + K_{eq}^{q(\mathrm{estim})}(T)C_0^q(\nu,T), \quad \text{(B.4)}$$

using the same pressure independent cross-sections $C_0^{b,q}(\nu,T)$ from Supplementary material 1 and *estimated* equilibrium constants given by dashed curves in Fig. 4:

$$K_{eq}^{b(estim)}(T) = 4.7856 \cdot 10^{-4} \cdot \exp\left(\frac{1662.20821}{T} - 5.87 \cdot 10^{-3} \cdot T\right), \quad \text{(B.5)}$$

$$K_{eq}^{q(estim)}(T) = 3.64986 \cdot 10^{-5} \cdot \exp\left(\frac{1788.16204}{T} + 2.48 \cdot 10^{-3} \cdot T\right). \quad \text{(B.6)}$$

Appendix C

Table C.1 – Description of the notation related to the equilibrium dimerization constant used here.

Notation	Quantity description	Details
K_{eq}^{b+q}	Temperature dependent physical quantity characterizing the content of H_2O dimers formed in a gas under equilibrium thermodynamic conditions.	$K_{eq}^{b+q} = \frac{P_{(H_2O)_2}}{P_{H_2O}^2}$, $K_{eq}^{b+q} = K_{eq}^{b} + K_{eq}^{q}$
$K_{eq}^{b+q(estim)}, K_{eq}^{b(estim)}$	Estimated values of K_{eq}^{b+q} and K_{eq}^{b}, known from independent calculations and experimental works.	$K_{eq}^{q(estim)} = K_{eq}^{b+q(estim)} - K_{eq}^{b(estim)}$
$K_{eq}^{b(fit)}, K_{eq}^{q(fit)}$	Fitted parameters of the water dimer model of the H_2O self-continuum [22]. These values are also expected to characterize the content of water dimers. However, given the incomplete understanding of the continuum nature, these values may differ from independent estimates $K_{eq}^{b(estim)}$ and $K_{eq}^{q(estim)}$.	$K_{eq}^{b+q(fit)} = K_{eq}^{b(fit)} + K_{eq}^{q(fit)}$
$K_{eq}^{b(mod)}, K_{eq}^{q(mod)}$	Fixed temperature dependent parameters of the new semi-empirical dimer-based continuum model, which provides a quantitative description of the water vapor continuum, regardless of its nature. These are the key quantities in this paper.	See the detailed description in Section 5 and Appendix B.

Data availability

Plot data are available upon request to the corresponding author.

Competing interests

The authors declare that they have no conflict of interest.

Acknowledgments

This work was performed under financial support from the Ministry of Science and Higher Education of the Russian Federation (Program of the Basic Scientific Investigations, budget funds for IAO SB RAS). In the early part of this work, KPS was funded by the UK Natural Environment Research Council grant, NE/R009848/1. The authors are grateful to Prof. Mikhail Tretyakov and Dr. Tatiana Galanina for valuable discussions.

Funding: This work was performed under financial support from the Ministry of Science and Higher Education of the Russian Federation (Program of the Basic Scientific Investigations, budget funds for IAO SB RAS,121031500297-3). In the early part of this work, KPS was funded by the UK Natural Environment Research Council grant, NE/R009848/1.

References

[1] Gordon IE, Rothman LS, Hargreaves RJ, Hashemi R, Karlovets E V., Skinner FM, et al. The HITRAN2020 molecular spectroscopic database. J Quant Spectrosc Radiat Transf 2022;277:107949. https://doi.org/10.1016/j.jqsrt.2021.107949.

[2] GEISA: Spectroscopic database n.d. https://geisa.aeris-data.fr/ (accessed August 7, 2024).

[3] Hettner G. Über das ultrarote Absorptionsspektrum des Wasserdampfes. Ann Phys 1918;360:476–96. https://doi.org/https://doi.org/10.1002/andp.19183600603.

[4] Clough SA, Iacono MJ, Moncet J-L. Line-by-Line calculation of atmospheric fluxes and cooling rates: application to water vapor. J Geophys Res 1992:15761–15785. https://doi.org/10.1029/92JD01419.

[5] Ptashnik I V., McPheat RA, Shine KP, Smith KM, Williams RG. Water vapor self-continuum absorption in near-infrared windows derived from laboratory measurements. J Geophys Res 2011;116:D16305(1-16). https://doi.org/10.1029/2011JD015603.

[6] Paynter D, Ramaswamy V. Variations in water vapor continuum radiative transfer with atmospheric conditions. J Geophys Res Atmos 2012;117:D16310(1-23). https://doi.org/10.1029/2012JD017504.

[7] Newman SM, Green PD, Ptashnik IV, Gardiner TD, Coleman MD, McPheat RA, et al. Airborne and satellite remote sensing of the mid-infrared water vapour continuum. Philos Trans R Soc A 2012;370:2611–36. https://doi.org/10.1098/rsta.2011.0223.

[8] Chesnokova TY, Firsov KM, Razmolov AA. Contribution of the water vapor continuum absorption to the radiation balance of the atmosphere with cirrus clouds. Atmos Ocean Opt 2019;32:64–71. https://doi.org/10.1134/S1024856019010056.

[9] Burch DE. Continuum Absorption By Atmospheric H2O. Proc SPIE 1981;277:28–39. https://doi.org/10.1117/12.931899.

[10] Burch DE. Absorption by H2O in narrow windows between 3000-4200 cm-1. US Air Force Geophys Lab Rep 1985:AFGL-TR-85-0036.

[11] Burch DE. Continuum absorption by H2O. AFGL-TR-81-0300 1982.

[12] Burch DE, Gryvnak DA. Method of calculating H2O transmission between 333 and 633 cm-1. Tech Rep AFGL-TR-79-0054, Air Force Geophys Lab, Hanscom AFB, Massachusetts 1979:1–50.

[13] Elsasser WM. Far infrared absorption of atmospheric water vapor. Astrophys J 1938;87:497–507. https://doi.org/10.1086/143940.

[14] Viktorova AA, Zhevakin SA. Absorption of micro-radiowaves in air by water vapor dimers. Rep Acad Sci USSR 1966;171:1061–1064.

[15] Penner SS, Varanasi P. Spectral absorption coefficient in the pure rotational spectrum of water vapor. J Quant Spectr Radiat Transf 1967;7:687–90. https://doi.org/10.1016/0022-4073(67)90024-6.

[16] Vigasin AA. Bimolecular absorption in atmospheric gases. Weakly Interact. Mol. Pairs Unconv. Absorbers Radiat. Atmos., Kluwer Academic Publishers; 2003, p. 23–48. https://doi.org/10.1007/978-94-010-0025-3_2.

[17] Vaida V, Daniel JS, Kjaergaard HG, Goss LM, Tuck AF. Atmospheric absorption of near infrared and visible solar radiation by the hydrogen bonded water dimer. Q J R Meteorol Soc 2001;127:1627–43. https://doi.org/10.1002/qj.49712757509.

[18] Ptashnik I, Smith K, Shine K, Newnham D. Laboratory measurements of water vapour continuum absorption in spectral region 5000–5600 cm-1: Evidence for water dimers. Q J R Meteorol Soc 2004;130:2391–2408. https://doi.org/10.1256/qj.03.178.

[19] Daniel JS, Solomon S, Kjaergaard HG, Schofield DP. Atmospheric water vapor complexes and the continuum. Geophys Res Lett 2004;31:L06118(1-4). https://doi.org/10.1029/2003gl018914.

[20] Paynter DJ, Ptashnik V, Shine KP, Smith KM. Pure water vapor continuum measurements between 3100 and 4400 cm-1: Evidence for water dimer absorption in near atmospheric conditions. Geophys Res Lett 2007;34:L12808. https://doi.org/10.1029/2007GL029259.

[21] Ptashnik IV. Evidence for the contribution of water dimers to the near-IR water vapour self-continuum. J Quant Spectrosc Radiat Transf 2008;109:831–852. https://doi.org/10.1016/j.jqsrt.2007.09.004.

[22] Ptashnik I, Shine KP, Vigasin AA. Water vapour self-continuum and water dimers : 1.Analysis of recent work. J Quant Spectrosc Radiat Transf 2011;112:1286–303. https://doi.org/10.1016/j.jqsrt.2011.01.012.

[23] Shine KP, Ptashnik I V., Rädel G. The Water Vapour Continuum: Brief History and Recent Developments. Surv Geophys 2012;33:535–55. https://doi.org/10.1007/s10712-011-9170-y.

[24] Ptashnik I V. Water vapour continuum absorption: Short prehistory and current status. Opt Atmos i Okeana 2015;28:443–59. https://doi.org/10.15372/AOO20150508.

[25] Ptashnik I V., Smith KM, Shine KP. Self-broadened line parameters for water vapour in the spectral region 5000-5600 cm-1. J Mol Spectrosc 2005;232:186–201. https://doi.org/10.1016/j.jms.2005.04.008.

[26] Odintsova TA, Tretyakov MY, Simonova AA, Ptashnik I V, Pirali O, Campargue A. Measurement and temperature dependence of the water vapor self-continuum between 70 and 700 cm−1. J Mol Struct 2020;1210:128046. https://doi.org/https://doi.org/10.1016/j.molstruc.2020.128046.

[27] Koroleva AO, Odintsova TA, Tretyakov MY, Pirali O, Campargue A. The foreign-continuum absorption of water vapour in the far-infrared (50–500 cm−1). J Quant Spectrosc Radiat Transf 2021;261:107486. https://doi.org/10.1016/j.jqsrt.2020.107486.

[28] Mlawer EJ, Cady-Pereira KE, Mascio J, Gordon IE. The inclusion of the MT_CKD water vapor continuum model in

the HITRAN molecular spectroscopic database. J Quant Spectrosc Radiat Transf 2023;306:108645. https://doi.org/10.1016/j.jqsrt.2023.108645.

[29] What's New 2023. https://github.com/AER-RC/MT_CKD_H2O/wiki/What's-New_H2O (accessed January 25, 2024).

[30] Simonova AA, Ptashnik IV. Water vapor self-continuum model in the rotational absorption band. Proc SPIE 2020;11560:1156002(1-7). https://doi.org/10.1117/12.2574937.

[31] Paynter DJ, Ptashnik I V., Shine KP, Smith KM, McPheat R, Williams RG. Laboratory measurements of the water vapor continuum in the 1200-8000 cm-1 region between 293 K and 351 K. J Geophys Res Atmos 2009;114:D21301(1-23). https://doi.org/10.1029/2008JD011355.

[32] Ptashnik I V., Klimeshina TE, Solodov AA, Vigasin AA. Spectral composition of the water vapour self-continuum absorption within 2.7 and 6.25 μm bands. J Quant Spectrosc Radiat Transf 2019;228:97–105. https://doi.org/10.1016/j.jqsrt.2019.02.024.

[33] Simonova AA, Ptashnik IV. Contribution of water dimers to the water vapor self-continuum absorption in fundamental bending and stretching bands. Atmos Ocean Opt 2022;35(2):110–7. https://doi.org/10.1134/S1024856022020117.

[34] Simonova AA, Ptashnik IV, Elsey J, McPheat RA, Shine KP, Smith KM. Water vapour self-continuum in near-visible IR absorption bands: Measurements and semiempirical model of water dimer absorption. J Quant Spectrosc Radiat Transf 2022;277:107957(1-17). https://doi.org/10.1016/j.jqsrt.2021.107957.

[35] Gordon IE, Rothman LS, Hill C, Kochanov R V, Tan Y, Bernath PF, et al. The HITRAN2016 molecular spectroscopic database. J Quant Spectrosc Radiat Transf 2017;203:3–69. https://doi.org/10.1016/j.jqsrt.2017.06.038.

[36] Mondelain D, Aradj A, Kassi S, Campargue A. The water vapour self-continuum by CRDS at room temperature in the 1.6 μm transparency window. J Quant Spectrosc Radiat Transf 2013;130:381–91. https://doi.org/10.1016/j.jqsrt.2013.07.006.

[37] Liebe HJ, Layton DH. Millimeter-wave properties of the atmosphere: Laboratory studies and propagation modeling. NTIA Rep 1987:87–224.

[38] Kuhn T, Bauer A, Godon M, Buehler S, Kuenzi K. Water vapor continuum: absorption measurements at 350 GHz and model calculations. J Quant Spectrosc Radiat Transf 2002;74:545–62. https://doi.org/https://doi.org/10.1016/S0022-4073(01)00271-0.

[39] Podobedov VB, Plusquellic DF, Siegrist KE, Fraser GT, Ma Q, Tipping RH. New measurements of the water vapor continuum in the region from 0.3 to 2.7 THz. J Quant Spectrosc Radiat Transf 2008;109:458–67. https://doi.org/10.1016/j.jqsrt.2007.07.005.

[40] Koshelev MA, Serov EA, Parshin VV, Tretyakov MY. Millimeter wave continuum absorption in moist nitrogen at temperatures 261 – 328 K. J Quant Spectr Radiat Transf 2011;112:2704–2712.

[41] Slocum D, Giles R, Goyette T. High-resolution water vapor spectrum and line shape analysis in the terahertz region.

J Quant Spectrosc Radiat Transf 2015;159:69–79. https://doi.org/10.1016/j.jqsrt.2015.03.006.

[42] Odintsova TA, Tretyakov MY, Pirali O, Roy P. Water vapor continuum in the range of rotational spectrum of H2O molecule: New experimental data and their comparative analysis. J Quant Spectrosc Radiat Transf 2017;187:116–23. https://doi.org/http://dx.doi.org/10.1016/j.jqsrt.2016.09.009.

[43] Koshelev MA, Leonov II, Serov EA, Chernova AI, Balashov AA, Bubnov GM, et al. New Frontiers in Modern Resonator Spectroscopy. IEEE Trans Terahertz Sci Technol 2018;8:773–83. https://doi.org/10.1109/TTHZ.2018.2875450.

[44] Odintsova TA, Tretyakov MY, Zibarova AO, Pirali O, Roy P, Campargue A. Far-infrared self-continuum absorption of H216O and H218O (15-500 cm-1). J Quant Spectrosc Radiat Transf 2019;227:190–200. https://doi.org/10.1016/j.jqsrt.2019.02.012.

[45] Tobin DC, Strow LL, Lafferty WJ, Olson WB. Experimental investigation of the self- and N2-broadened continuum within the ν2 band of water vapor. Appl Opt 1996;35:4724. https://doi.org/10.1364/ao.35.004724.

[46] Ptashnik I V., Petrova TM, Ponomarev YN, Shine KP, Solodov AA, Solodov AM. Near-infrared water vapour self-continuum at close to room temperature. J Quant Spectrosc Radiat Transf 2013;120:23–35. https://doi.org/10.1016/j.jqsrt.2013.02.016.

[47] Ptashnik IV, Klimeshina TE, Petrova TM, Solodov AA, Solodov AM. Water Vapor Continuum Absorption in the 2.7 and 6.25 μm Bands at Decreased Temperatures. Atmos Ocean Opt 2016;29:211–5. https://doi.org/10.1134/S1024856016030131.

[48] Birk M, Wagner G, Loos J, Shine KP. 3 μm Water vapor self- and foreign-continuum: New method for determination and new insights into the self-continuum. J Quant Spectrosc Radiat Transf 2020;253:107134. https://doi.org/10.1016/j.jqsrt.2020.107134.

[49] Mitsel' AA, Ptashnik I V., Firsov KM, Fomin BA. Efficient technique for line-by-line calculating the transmittance of the absorbing atmosphere. Atmos Ocean Opt 1995;8:1547–51. https://doi.org/10.1016/0022-4073(95)00029-K.

[50] Clough SA, Kneizys FX, Davies RW. Line shape and the water vapor continuum. Atmos Res 1989;23:229–41. https://doi.org/https://doi.org/10.1016/0169-8095(89)90020-3.

[51] Klimeshina TE, Ptashnik IV. Software for retrieving the water vapor continuum absorption from experimental data. Atmos Ocean Opt 2018;31:451–456. https://doi.org/10.1134/S1024856018050093.

[52] Schofield DP, Kjaergaard HG. Calculated OH-stretching and HOH-bending vibrational transitions in the water dimer. Phys Chem Chem Phys 2003;5:3100–5. https://doi.org/10.1039/b304952c.

[53] Curtiss LA, Frurip DJ, Blander M. Studies of molecular association in H2O and D2O vapors by measurement of thermal conductivity. J Chem Phys 1979;71:2703–2711. https://doi.org/10.1063/1.438628.

[54] Vigasin AA. Bound, metastable and free states of bimolecular complexes. Infrared Phys 1991;32:451–70. https://doi.org/10.1016/0020-0891(91)90135-3.

[55] Stogryn DE, Hirschfelder JO. Contribution of bound, metastable, and free molecules to the second virial coefficient

and some properties of double molecules. J Chem Phys 1959;31:1531–45. https://doi.org/10.1063/1.1730649.

[56] Vigasin AA. On the possibility to quantify contributions from true bound and metastable pairs to infrared absorption in pressurised water vapour. Mol Phys 2010;108:2309–13. https://doi.org/10.1080/00268971003781563.

[57] Kjaergaard HG, Garden AL, Chaban GM, Gerber RB, Matthews DA, Stanton JF. Calculation of vibrational transition frequencies and intensities in water dimer: Comparison of different vibrational approaches. J Phys Chem A 2008;112:4324–35. https://doi.org/10.1021/jp710066f.

[58] Kuyanov-Prozument K, Choi MY, Vilesov AF. Spectrum and infrared intensities of OH-stretching bands of water dimers. J Chem Phys 2010;132:014304(1-7). https://doi.org/10.1063/1.3276459.

[59] Tretyakov MY, Serov EA, Odintsova TA. Equilibrium thermodynamic state of water vapor and the collisional interaction of molecules. Radiophys Quantum Electron 2012;54:700–16. https://doi.org/10.1007/s11141-012-9332-x.

[60] Ruscic B. Active thermochemical tables: Water and water dimer. J Phys Chem A 2013;117:11940–53. https://doi.org/10.1021/jp403197t.

[61] Leforestier C. Water dimer equilibrium constant calculation: A quantum formulation including metastable states. J Chem Phys 2014;140:074106. https://doi.org/10.1063/1.4865339.

[62] Scribano Y, Goldman N, Saykally RJ, Leforestier C. Water Dimers in the Atmosphere III : Equilibrium Constant from a Flexible Potential. J Phys Chem A 2006;110:5411–9. https://doi.org/10.1021/jp056759k.

[63] Buryak I, Vigasin AA. Classical calculation of the equilibrium constants for true bound dimers using complete potential energy surface. J Chem Phys 2015;143:234304(1-8). https://doi.org/10.1063/1.4938050.

[64] Rocher-Casterline B, Ch'ng L, Mollner A, Reisler H. Communication: determination of the bond dissociation energy (D0) of the water dimer, (H2O)2, by velocity map imaging. J Chem Phys 2011;134:211101(1-4). https://doi.org/10.1063/1.3598339.

[65] Serov EA, Odintsova TA, Tretyakov MY, Semenov VE. On the origin of the water vapor continuum absorption within rotational and fundamental vibrational bands. J Quant Spectrosc Radiat Transf 2017;193:1–12. https://doi.org/10.1016/j.jqsrt.2017.02.011.

[66] Scribano Y, Leforestier C. Contribution of water dimer absorption to the millimeter and far infrared atmospheric water continuum. J Chem Phys 2007;126:1–12. https://doi.org/10.1063/1.2746038.

[67] Lee M-S, Baletto F, Kanhere DG, Scandolo S. Far-infrared absorption of water clusters by first-principles molecular dynamics. J Chem Phys 2008;128:214506. https://doi.org/10.1063/1.2933248.

[68] Vogt E, Kjaergaard HG. Vibrational spectroscopy of the water dimer at jet-cooled and atmospheric temperatures. Annu Rev Phys Chem 2022;73:209–31. https://doi.org/10.1146/annurev-physchem-082720-104659.

[69] Vogt E, Simkó I, Császár AG, Kjaergaard HG. Reduced-dimensional vibrational models of the water dimer. J Chem Phys 2022;156. https://doi.org/10.1063/5.0090013.

[70] Vogt E, Simko I, Császár AG, Kjaergaard HG. Quantum chemical investigation of the cold water dimer spectrum in the first OH-stretching overtone region provides a new interpretation. J Phys Chem A 2023;127:9409–18.

https://doi.org/10.1021/acs.jpca.3c03705.

[71] Bouteiller Y, Perchard JP. The vibrational spectrum of (H2O)2: comparison between anharmonic ab initio calculations and neon matrix infrared data between 9000 and 90 cm−1. Chem Phys 2004;305:1–12. https://doi.org/https://doi.org/10.1016/j.chemphys.2004.06.028.

[72] Slipchenko MN, Kuyanov KE, Sartakov BG, Vilesov AF. Infrared intensity in small ammonia and water clusters. J Chem Phys 2006;124:241101(1-4). https://doi.org/10.1063/1.2216712.

[73] Salmi T, Hänninen V, Garden AL, Kjaergaard HG, Tennyson J, Halonen L. Calculation of the O - H stretching vibrational overtone spectrum of the water dimer. J Phys Chem A 2008;112:6305–12. https://doi.org/10.1021/jp800754y.

[74] Salmi T, Hänninen V, Garden AL, Kjaergaard HG, Tennyson J, Halonen L. Correction to "Calculation of the O-H stretching vibrational overtone spectrum of the water dimer." J Phys Chem A 2012;116:796–7. https://doi.org/10.1021/jp210675h.

[75] Ivanov SV. Trajectory study of CO2–Ar and CO2–He collision complexes. In: Camy-Peyret C, Vigasin AA, editors. Weakly Interact. Mol. pairs Unconv. absorbers Radiat. Atmos., Netherlands: Kluwer Academic Publishers; 2003, p. 49–63.

[76] Kojić D, Simonova AA, Yasui M. Removal of the ambient air features from fourier-Transform near-Infrared spectra. J Quant Spectrosc Radiat Transf 2023;301:108538. https://doi.org/10.1016/j.jqsrt.2023.108538.